

Article

Discovery of 178 Giant Radio Galaxies in 1059 deg² of the Rapid ASKAP Continuum Survey at 888 MHz

Heinz Andernach ^{1,*}, Eric F. Jiménez-Andrade ² and Anthony G. Willis ³

¹ Departamento de Astronomía, DCNE, Universidad de Guanajuato, Callejón de Jalisco s/n, Guanajuato C.P. 36023, GTO, Mexico

² National Radio Astronomy Observatory, 520 Edgemont Road, Charlottesville, VA 22903, USA; ejimenez@nrao.edu

³ Independent Researcher, 310 Yorkton Avenue, Penticton, BC V2A 6Z8, Canada; tony.willis.research@gmail.com

* Correspondence: heinz@ugto.mx

Abstract: We report the results of a visual inspection of images of the Rapid ASKAP Continuum Survey (RACS) in search of extended radio galaxies (ERG) that reach or exceed linear sizes on the order of one Megaparsec. We searched a contiguous area of 1059 deg² from RA_J = 20^h20^m to 06^h20^m, and −50° < Dec_J < −40°, which is covered by deep multi-band optical images of the Dark Energy Survey (DES) and in which previously only three ERGs larger than 1 Mpc had been reported. For over 1800 radio galaxy candidates inspected, our search in optical and infrared images resulted in hosts for 1440 ERG, for which spectroscopic and photometric redshifts from various references were used to convert their largest angular size (LAS) to projected linear size (LLS). This resulted in 178 newly discovered giant radio sources (GRS) with LLS > 1 Mpc, of which 18 exceed 2 Mpc and the largest one is 3.4 Mpc. Their redshifts range from 0.02 to ~2.0, but only 10 of the 178 new GRS have spectroscopic redshifts. For the 146 host galaxies, the median *r*-band magnitude and redshift are 20.9 and 0.64, while for the 32 quasars or candidates these are 19.7 and 0.75. Merging the six most recent large compilations of GRS results in 458 GRS larger than 1 Mpc, so we were able to increase this number by ~39% to 636.

Keywords: galaxies; radio sources; optical identification; giant radio galaxies; radio surveys



Citation: Andernach, H.; Jiménez-Andrade, E.F.; Willis, A.G. Discovery of 178 Giant Radio Galaxies in 1059 deg² of the Rapid ASKAP Continuum Survey at 888 MHz. *Galaxies* **2021**, *9*, 99. <https://doi.org/10.3390/galaxies9040099>

Academic Editors: Francesca Loi and Tiziana Venturi

Received: 30 September 2021

Accepted: 2 November 2021

Published: 9 November 2021

Publisher's Note: MDPI stays neutral with regard to jurisdictional claims in published maps and institutional affiliations.



Copyright: © 2021 by the authors. Licensee MDPI, Basel, Switzerland. This article is an open access article distributed under the terms and conditions of the Creative Commons Attribution (CC BY) license (<https://creativecommons.org/licenses/by/4.0/>).

1. Introduction

Giant radio galaxies (GRG) were first discovered in 1974 [1] and were originally defined as those for which their projected linear size (LLS) exceeds 1 Mpc, at a time when the Hubble constant was assumed to be $H_0 = 50 \text{ km s}^{-1} \text{ Mpc}^{-1}$. Today, H_0 is accepted to be near $70 \text{ km s}^{-1} \text{ Mpc}^{-1}$ so that objects of the same angular size now have a linear size smaller by a factor of ~1.4. Thus the first GRG found (3C 236) originally assigned an LLS of 5.7 Mpc, is now considered to extend over 4.1 Mpc. This change in the adopted value of H_0 has led more recent authors to adopt an LLS of 0.7 Mpc as a lower limit for considering a radio galaxy a “giant” one. However, there is no physical reason for adopting either of these thresholds, and in the present paper, we focus on only those larger than 1 Mpc.

In 1983 [2] the first two giant radio quasars (GRQs) were found, [HB89] 1146–037 of LLS = 1.06 Mpc, at a redshift of $z = 0.341$, and [HB89] 1429 + 160 with 1.37 Mpc at $z = 1.016$, and these authors already raised the issue that inverse Compton losses suffered by the synchrotron-emitting electrons by scattering the cosmic microwave background (CMB) photons at $z \gtrsim 1$, and the denser Universe at that cosmic epoch, should not let these GRQs expand to the same extent as in the local Universe. Since then, many other GRQs have been found, and currently they constitute about 18% of all known giant radio sources (GRS); see also Section 4.1. Unless otherwise noted, here we use the terms GRS, GRG, and GRQ for sources with LLS > 1 Mpc.

Despite an intense search for farther and larger examples of these rare objects, only two GRGs larger than 3C 236 have been found so far, namely J1420–0545 of 4.7 Mpc [3] and J0931 + 3204 of 4.3 Mpc [4], the latter being the largest GRQ currently known. A third GRG of supposedly 4.45 Mpc, listed as J1234 + 5318 in the latest GRS compilation by [5], was originally published by [6] but was later shown to have a lower-redshift host on the basis of a deeper image from the Low Frequency Array (LOFAR) [7], which led to a smaller LLS of 3.25 Mpc. This latter object, with a largest angular size (LAS) of $\sim 11'$, is an interesting example of the difficulty to correctly identify the host of a radio galaxy with widely spaced lobes.

As shown by [1,8], while GRGs are not the most radio-luminous extragalactic radio sources, they tend to have the lowest minimum energy densities (down to $\sim 10^{-14}$ J m $^{-3}$) in relativistic particles and magnetic field, and, due to their huge volume, they have the largest total energy content in particles and magnetic field, up to a few times 10^{54} J, and as such, as expressed by [9], “put the greatest strain on radio source models”.

Until recently, the search for GRS was mainly based on two large-scale radio surveys, the NRAO VLA Sky Survey (NVSS, [10]) with an angular resolution of $45''$ and sensitive to the diffuse emission from radio galaxy lobes, and the Faint Images of the Radio Sky at Twenty centimeters (FIRST, [11]), which, due to its higher angular resolution of $5.4''$, best reveals the radio nuclei and thus the host position of extended sources. Both surveys were carried out at 1.4 GHz with the Very Large Array (VLA) in New Mexico, USA, which has led to the fact that the majority of known GRS were found in the northern celestial hemisphere, which is also largely covered by deep imaging and spectroscopic surveys such as the Sloan Digital Sky Survey (SDSS, [12]). Thus, the latest literature compilation [5] lists 213 GRS, of which 20 (9.4%) lie south of Dec = -40° , an area of 17.9% of the sky. Only recently, with the advent of sensitive low-frequency surveys such as the LOFAR Two-metre Sky Survey (LoTSS, [13]) and those performed with the Australian Square Kilometre Array Pathfinder (ASKAP, see [14]) more GRS are being found in both hemispheres [15–17].

In order to increase the number of known GRS, especially in the far southern hemisphere (Dec < -40°), we explore here the possible content of GRS in the recent Rapid ASKAP Continuum Survey (RACS, [18]), which has imaged 83% of the entire sky (Dec < $+41^\circ$) at 888 MHz with an angular resolution of $15''$ and an average noise level of 0.25 mJy beam $^{-1}$. Both characteristics are three times better than those of the previously best southern radio survey, the Sydney University Molonglo Sky Survey (SUMSS, [19,20]). This makes RACS the first radio survey to cover the far southern sky that allows us to identify the hosts of the majority of extended radio sources in modern optical/IR surveys like SkyMapper (SMSS, [21]), the Dark Energy Survey (DES, [22]), and those of the Wide-field Infrared Survey Explorer (WISE, e.g., [23,24]).

As already found by [25], the often cited reasons for the extreme sizes acquired by GRS, namely (i) a preferred orientation in the plane of the sky, (ii) a location in lower-density environments, and (iii) more powerful jets feeding their lobes, cannot explain the observations, and these authors argue that a more likely reason is a much longer duration of their radio-active phase, although the latter is difficult to prove. Further motivations for a continued search for GRS are (a) the question of whether there is a physical limit near ~ 5 Mpc for GRS and (b) to use them as probes of the large-scale structure of the Universe, since [26,27] have shown, albeit on a limited sample of relatively nearby GRS, that the major axes connecting the two lobes of GRS have a tendency to lie perpendicular to the orientation of the ambient galaxy overdensity or that of galaxy filaments of which the host is a member. A list of extended RGs of any size but with a high surface density per deg 2 would also be useful to test conjectures of alignments of their radio position angles like those claimed by [28,29]. Eventually, we were also interested in finding out how well a relatively low angular resolution survey like RACS and the imminent all-sky survey “Evolutionary Map of the Universe” (EMU [17]) would be suited to unambiguously identify the hosts of extended radio sources.

In this paper, we adopt standard cosmological parameters of $H_0 = 70 \text{ km s}^{-1} \text{ Mpc}^{-1}$, $\Omega_m = 0.3$, $\Omega_\Lambda = 0.7$, and a radio source spectral index α defined as $S_\nu \propto \nu^\alpha$.

2. Methodology

Given that [30] had screened the then-existing SUMSS images for GRS in an area of 2100 deg^2 (defined by $\text{Dec}_J < -50^\circ$ and Galactic latitude $|b| > 12.5^\circ$) and had found 21 objects with $\text{LAS} > 5'$, later published in [31], we selected for the first systematic search for GRS in RACS with a declination range from -40° to -50° . Knowing that radio galaxies tend to be found up to high redshifts, implying very faint hosts, we further limit ourselves to the high Galactic latitude area from $\text{RA} = 20^{\text{h}}20^{\text{m}}$ to $06^{\text{h}}20^{\text{m}}$ (a total of 1059 deg^2), as it is covered by DES, providing deep optical g, r, i -band images and photometric redshifts. The literature compilation by [5] lists only three GRS in this area.

Small parts of this area had been surveyed previously in radio, and the corresponding images had been inspected by one of us (H.A.) for the presence of GRS. Firstly, the Australia Telescope ESO Slice Project (ATESP, [32]), covering $\text{RA}_J = 22^{\text{h}}32^{\text{m}}\text{--}22^{\text{h}}57^{\text{m}}$ and $23^{\text{h}}31^{\text{m}}\text{--}01^{\text{h}}23^{\text{m}}$ in the range $-39.5^\circ < \text{Dec}_J < -40.4^\circ$, overlaps for $\sim 17 \text{ deg}^2$ with our search area. Secondly, a circular area of $\sim 4.5 \text{ deg}^2$ had been imaged with the Australia Telescope Compact Array (ATCA) at 1.4 GHz as the Phoenix Deep Field (PDS) [33,34] centered on $\text{RA}_J, \text{Dec}_J = 01^{\text{h}}13^{\text{m}}36^{\text{s}}, -45.7^\circ$. Thirdly, an area of $\sim 40 \text{ deg}^2$ ($\text{RA}_J = 20^{\text{h}}05^{\text{m}}\text{--}22^{\text{h}}26^{\text{m}}, -48.1^\circ < \text{Dec}_J < -50^\circ$) overlaps with our search region and had been imaged with ASKAP as part of the EMU Pilot Survey [17] at the same angular resolution as RACS, but to a $1\text{-}\sigma$ noise level 10 times lower ($\sim 26 \mu\text{Jy beam}^{-1}$). We include in our results only those GRS that can be recognized on RACS images.

2.1. Images Used

For our visual inspection, we used the RACS images for Stokes I data release 1, available in full resolution from https://www.atnf.csiro.au/research/RACS/RACS_I1 (accessed on 20 September 2021). The beam size and shape of the latter images vary with sky position [35] such that the beam major axes range from $15''$ to $25''$. The RACS Stokes I data release 1 images are also provided as “CRACS”, convolved to a common resolution of $25''$ at the URL https://www.atnf.csiro.au/research/RACS/CRACS_I2 (accessed on 20 September 2021), which were used to prepare the source catalogue in [35]. Both versions are in J2000 coordinates, and pixel intensities are calibrated in Jy beam^{-1} . For our search for GRS, we preferred the full-resolution images to better constrain the most likely host position, but occasionally consulted CRACS to confirm the presence of diffuse emission. The astrometric precision of RACS is better than $1''$ [18,35] and thus does not affect the reliability of optical identifications. It is rather the angular resolution that causes an increased rms of the source position, which amounts to $\sim 2.7''$ for a faint source of $\text{S/N} \sim 5$ [18].

During a summer internship in 2012 at Univ. of Guanajuato, one of us (E.F.J.-A.), together with R.F. Maldonado Sánchez [36], had inspected all of the SUMSS images, logging the positions of ~ 5000 potentially extended radio sources. Since then, a fraction of these have been followed up by one of us (H.A.) to either optically identify their host or discard them as unrelated sources. However, the low angular resolution of SUMSS ($45''$), together with the limited sensitivity of the optical Digitized Sky Survey [37], often made this task a guesswork, and only the advent of RACS in radio and DES in the optical promised a solution. Thus, in the first round of our search for GRS, we inspected RACS images at a few hundred previously logged positions in our search area. We used ALADIN ([38], <http://aladin.u-strasbg.fr/aladin.gml> (accessed on 10 June 2021)) to display these images, adjusting the contrast such that the noise floor could always be recognized. Whenever the source structure in RACS appeared as two or more unrelated sources, they were discarded, and otherwise the g, r, i -composites of optical images from DES were consulted to find the most likely host, and its position was recorded for later retrieval of complementary data. Over 260 radio sources spotted in SUMSS were thus identified with the help of RACS.

In the second round, we systematically screened the full area of 1059 deg^2 in the full-resolution RACS, marking on it with symbols those sources already identified in the first round, as well as apparently extended sources that had been discarded previously, so as to avoid repeating the identification process for these.

Given that our aim was to find, apart from GRS, also those with an appreciable size of $\text{LLS} \gtrsim 0.5 \text{ Mpc}$, we tried to log all possible sources with a $\text{LAS} \gtrsim 1.0'$, since for our adopted cosmology this is the minimum angular size a standard ruler of 0.5 Mpc would appear if it had a redshift in the range of $\sim 1.4\text{--}1.8$ (see, e.g., Figure 30 on p. 1326 of [39] and our $\text{LAS} - z$ diagram in Section 4.1. We also included, though less complete for $\text{LAS} \lesssim 1.5'$, bent-tailed radio sources like wide-angle tailed (WAT) and narrow-angle tailed (NAT) sources, since these may serve as indicators of the presence of a cluster of galaxies. We proceeded from $\text{RA} = 20^{\text{h}}20^{\text{m}}$ eastward by scanning portions 1 h wide in RA (or $\sim 100 \text{ deg}^2$ at the chosen declination), displaying about 1 deg^2 per screen at a time and logging between 1 and 1.5 candidates per deg^2 , which took about 16 h for the entire 1059 deg^2 . This resulted in a list of approximate center positions of ~ 1330 candidate extended radio sources.

2.2. Scrutinizing the Candidates: Host Identification and Radio Morphology

The positions of all the ~ 1330 candidates selected in the previous step were then displayed again in ALADIN, and the likely host was searched on DES DR1 g, r, i -band color composites [22]. DES DR1 has a median delivered point-spread function of 1.12, 0.96, and $0.88''$ in the g, r , and i -bands, an astrometric precision of $0.151''$, and limiting magnitudes of 24.28, 23.95, and 23.34 mag in g, r , and i -bands for objects with $\text{S/N} = 10$ and a $2''$ -diameter aperture. We also used mid-infrared (MIR) images from unWISE [24], colored according to the magnitude difference between the two lowest-wavelength WISE bands, $W1 - W2$. For sources with an obvious central radio core, finding the host object was easy, both for the edge-darkened Fanaroff–Riley [40] type I (or FRI) sources with a radio brightness peak close to the optical host, and for the edge-brightened FR II sources with a radio core. The problem arises for sources with widely separated radio components and without an obvious central component in between them. If the central component had no optical or MIR counterpart, the pair of outer components was discarded as a genuine RG. However, if one of the outer components had a convincing host by itself and its radio extent was larger than $\sim 1'$, it was recorded as a separate extended RG. If the central component had a clear optical or MIR host, the candidate was discarded if the outer components had an obvious counterpart, unless their radio structure showed clear indications of being connected (e.g., radio bridges or trails pointing at each other) and the optical/MIR objects in the lobes did not show evidence for being active galactic nuclei (AGN). When deemed necessary, RACS radio contours were drawn interactively in ALADIN and overlaid on DES and/or unWISE images. The unWISE images were especially helpful in suggesting a likely host for sources with widely separated lobes without an obvious radio nucleus and without a prominent galaxy or quasar near their geometrical center. Occasionally the unWISE images helped us to decide between two optical counterparts very close to each other. In cases of lobes with very different radio brightness, a higher probability was assigned to hosts nearer to the brighter lobe (cf. [41]). Whenever the optical hosts were too faint or uncatalogued in DES DR1, we consulted the Dark Energy Spectroscopic Instrument (DESI, [42]) DR9 images at <https://www.legacysurvey.org> (accessed on 20 September 2021) and usually found the corresponding DESI object and its r -band magnitude. In case of doubt about the likely host, we generally chose the brighter or lower-redshift host, such that the derived LLS should serve as a lower limit.

Often the likely optical hosts, or objects superposed on the suspected lobes, appeared stellar, either by visual impression or confirmed by the stellarity index provided in the DES DR1 catalogue. To distinguish between stars and quasars, we made use of both the measurements of parallax and proper motion in the Global Astrometric Interferometer for Astrophysics (Gaia) early data release 3 (Gaia EDR3, [43]), which should be consistent with zero for quasars, as well as their $W1 - W2$ and $W2 - W3$ colors in the AllWISE

catalogue [23,44] Based on this information, we discarded the likely stars as possible radio galaxy hosts or else labeled the host as quasar candidate or “Qc” in Table 2. We also took note of any optical peculiarities of the host-like stellar/QSO or spiral morphology, presence of optical shells, interactions or perturbations, etc.

Obvious relic-type radio sources in clusters of galaxies, not associated with any single cluster galaxy, as well as nearby late-type spiral galaxies, were discarded as radio galaxy candidates. We maintained a few possible candidates for so-called spiral double radio galaxy AGN (SDRAGN [45]), though all of these had linear sizes $\ll 1$ Mpc.

During this inspection, we also measured the LAS for each accepted candidate and classified its radio morphology into one or more types as listed in Table 1, appended by a “?” symbol to indicate uncertainty. We avoided any systematic overestimate of the LAS; e.g., for FR II sources with bright hotspots, we did not measure the LAS between opposite $3\text{-}\sigma$ contours but rather between the centres of the outer half-circles of these contours of each hotspot. Only for rather faint or diffuse lobes we measured out to about the $3\text{-}\sigma$ contours (see [46] Section 2 for a discussion of LAS measures). For bent-tailed sources, we measured the LAS along a straight line between the most separate diametrically opposite emission regions of the source and not along their curved emission ridges.

Table 1. List of radio-morphological types we assigned to our sources.

Morph.Type	Description
FRI	radio brightness is “edge-darkened”, fading away with distance from the host
FR II	classical double with “edge-brightened” outer lobes
FRI/II	source shows characteristics of both FRI and FR II
FRIIncor	widely separated double with no obvious radio core at the optical host
FRIIcoredom	radio nucleus very strong compared to the lobes
FRIInaked	no evidence for radio trails or bridges: lobes are unresolved hotspots
FRIIplume(s)	diffuse emission regions displaced sideways from source major axis
FRIIrelic	lobes slightly diluted
FRIIremn	lobes very diluted/inflated and of low surface brightness
DDRG	double-double or “restarted” radio galaxy: an inner and outer pair of lobes
hymor	hybrid morphology: one arm or lobe is of type FRI, the other type FR II
WAT	wide-angle tailed RG with outer lobes bent in the same direction, C-shaped
NAT	narrow-angle tailed RG: host galaxy is located at one end of radio emission
precess	Z- or S-symmetry, suggesting precession of the radio jet axis
asym	length or flux ratio of opposite lobes is near two or more

Scrutinizing these ~ 1330 candidates required ~ 40 net hours and led us to discard $\sim 30\%$ of them, resulting in a list of precise host positions, LAS measures, and a crude radio-morphological classification for ~ 1000 extended radio sources, in addition to the ~ 260 objects initially suspected on SUMSS images and confirmed by us in RACS.

2.3. Culling Complementary Data for the Radio Galaxy Hosts

We first queried the positions of the ~ 1300 newly discovered ERG hosts from RACS in the NASA/IPAC Extragalactic Database (NED, ned.ipac.caltech.edu (accessed on 30 August 2021)) to find spectroscopic redshifts for 68 of them, mostly among the optically brightest hosts. We then used the VizieR service at the Strasbourg astronomical Data Center (CDS, [47]) at the URL <https://vizier.u-strasbg.fr/viz-bin/VizieR> (accessed on 30 August 2021) to search for host names and complementary data for these hosts. For all hosts, we searched names (if available) from the 2MASX catalogue [48] (CDS VII/233), their exact positions, names, and r -band magnitudes, as well as stellarity index from DES DR1 [22] (CDS I/357), and the WISEA names and magnitudes in all four WISE bands from AllWISE [23] (CDS II/328), as well as W1 and W2 magnitudes from the deeper CatWISE2020 [49] (CDS II/365).

2.4. Photometric Redshifts and Conversion from Angular to Linear Size

We used several different sources outside VizieR for photometric redshifts (z_{phot}).

For 2MASX galaxies, we searched the 2MASS Photometric Redshift catalogue (2MPZ, [50]) and the hosts found in AllWISE [23] were searched in the WISE-Supercosmos photometric redshift catalogue [51] offering 20.4 and 57.9 million objects in the “main” and “reject” catalogues, respectively. Previous experience showed that the z_{phot} from the “reject” catalogue are mostly sound and were used as well.

The z_{phot} values offered by DESI DR9 [52] were extracted from the DESI Legacy Survey DR9 through the Notebook Server of the NOIRLab Data Lab Query Interface at <https://datalab.noirlab.edu/query.php> (accessed on 10 June 2021). Since DESI DR9 data are stored in different tables, we cross-matched the main photometry table (ls_dr9.tractor) and the one with photometric redshifts (ls_dr9.photo_z) via the objectID searching for a radius of $2''$ from the host position and requesting object coordinates, g, r, z -magnitudes, and median and mean z_{phot} . For a few objects, the z_{phot} values from DESI DR9 were obtained directly at viewer.legacysurvey.org (accessed on 20 August 2021).

The DESI DR9 z_{phot} catalogue also lists the standard deviation (which we call Δz here) of the the z_{phot} probability distribution function. We found the latter to be $\Delta z \sim 0.01$ below $z_{phot} \sim 0.4$, gradually rising to $\Delta z \sim 0.05$ near $z_{phot} \sim 0.8$ and to $\Delta z \sim 0.15$ for $z_{phot} \gtrsim 1.0$. For 23 (13%) of our new 178 GRS in Table 2, the Δz values exceed 0.17 and reach up to 0.6, but these objects are predominantly QSO candidates (for which we use additional z_{phot} estimates, see below) and some very faint galaxies. For 41 GRS up to a redshift of ~ 0.6 , we had z_{phot} values from both DESI DR9 and [51]. The difference (DESI DR9 minus [51]) has a mean of 0.03 and a standard deviation of 0.09. Averaging the latter values should further reduce their uncertainty. Although the z_{phot} values are considerably more uncertain at higher redshift, the LLS is much less sensitive to the redshift for a given LAS at redshifts between 1 and 2 (see our Figure 6).

It is known that for QSOs it is notoriously difficult to estimate redshifts, and a large fraction of starlike QSO candidates among our hosts have clearly underestimated z_{phot} values in DES DR1. For some of them, we found estimated redshifts in [53], and, in addition, for all our quasar candidates, we use MIR colors $W1 - W2$ and $W2 - W3$ from AllWISE where available and consulted Figure 2 of [54] to estimate their redshift. We combined all the redshifts found and adopted a reasonable average of these if more than one was available and provide these in Table 2.

In order to find the physically largest objects in our sample, we converted the sources' LAS to their LLS, using a script adapted from the Cosmology Calculator ([55], <http://www.astro.ucla.edu/~wright/CosmoCalc.html> (accessed on 15 September 2021)), and based on the adopted redshift (z_{spec} or z_{phot}) and cosmological parameters as listed at the end of Section 1. We stress that the LLS is always a lower limit to the 3-D extent of the source, and we make no inference about its orientation with respect to the line of sight as done, e.g., in [56].

2.5. Determination of Radio Flux Densities and Luminosities

Cutouts of at least $2 \times$ LAS on a side were obtained for each source from both RACS and CRACS using a script as suggested at <http://alaska.u-strasbg.fr/hips-image-services/hips2fits> (accessed on 20 August 2021). These were then passed through the breizorro masking program (see <https://github.com/ratt-ru/breizorro> (accessed on 20 August 2021)), which creates a binarized image assigning a value of 1 to every pixel brighter than $n\sigma$, where σ is the noise level and values of 0 elsewhere. By trial and error, we found that a $3\text{-}\sigma$ threshold worked best.

These binarized images were then run through the python matplotlib program, which calculates contours around the areas assigned a value of 1 and then colors the boundaries of the ten contours containing the largest areas. These are usually the ones containing the real source confines, plus occasional unrelated sources, but sometimes an isolated central nuclear source could have a contour area smaller than the ten largest.

The contour areas considered to contain the emission from the extended radio source are then selected manually (by clicking the mouse on these) to be run through the source parameter analysis. Usually, we selected between two such areas (e.g., for a source with only two lobes and no radio core) and up to about five such areas (e.g., for a source with a radio core and two separated emission areas for each lobe on opposite sides of the host), but occasionally the presence of a radio core and emission bridge connecting the lobes leads to the source being contained in a single such area.

The pixels making up the individual contour boundaries, along with the x, y positions inside contours that were selected in the previous operation, are then passed to the script that calculates source parameters. It first multiplies the original image by the `breizorro` mask. For a selected contour, it then sums up the brightness values of all pixels inside a contour and finally normalizes by the number of pixels per beam solid angle to obtain the flux density within a particular contour. To figure out which pixels lie inside a contour, the python package `Shapely` (see <https://github.com/Toblerity/Shapely> (accessed on 20 August 2021)) was used. A contour equates to a polygon in `Shapely`, which can generate a `MultiPolygon` from a collection of polygons. `Shapely` is also used to find out which contours are to be used in the analysis by determining which contours contain the x, y positions determined by the mouse clicks in the previous step. This allows one to calculate total flux densities, largest angular size, etc., which in fact we use to estimate magnetic field strength and energy densities for the individual lobes based on the assumption of equipartition between particle and magnetic field energies (see [57]). However, for the present paper, we limit ourselves to report only the total flux of each source, as well as the position angle of the radio source's major axis.

As a final step, we compared the total flux densities obtained from RACS and CRACS to select the most adequate total flux, avoiding as much as possible the contributions of unrelated sources, and these are listed as S_{888} in Table 2. Rest-frame spectral radio powers at 888 MHz were then obtained via $P_{888} = 4\pi D_L^2(z) S_{888} (1+z)^{-(1+\alpha)}$, where $D_L(z)$ is the luminosity distance for the adopted cosmology and $(1+z)^{-(1+\alpha)}$ is the k -correction to convert from observed to rest frequency and allows for the stretching of the spectrum with respect to the receiver bandwidth. In the absence of measured spectral indices, we assume $\alpha = -0.8$, which is slightly steeper than the average spectrum of radio galaxies of $\alpha = -0.7$ [58], given that we are dealing mostly with objects dominated by emission from diffuse radio lobes. We list the decimal logarithm of P_{888} in Table 2.

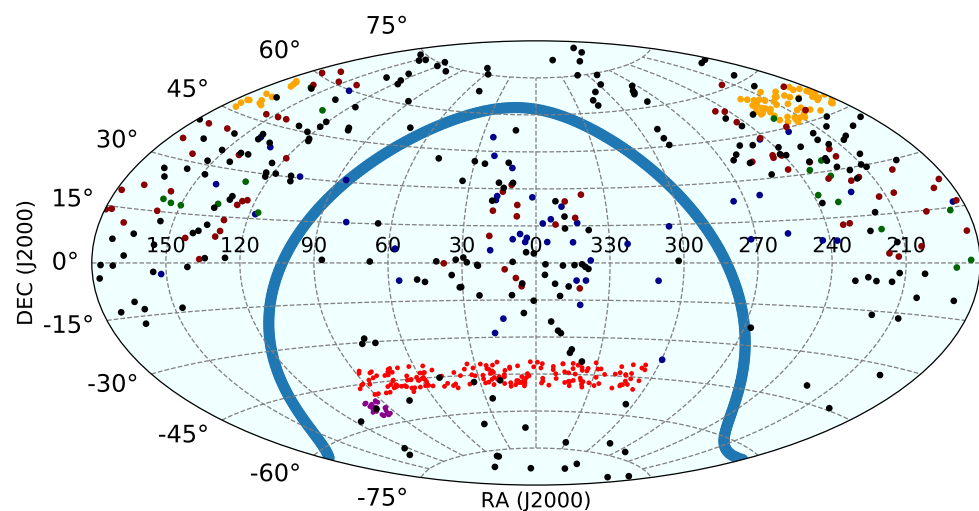


Figure 1. All-sky Aitoff projection of the distribution of our newly discovered GRS in red, together with the GRS from six major published GRS lists, which are in black from [5], in orange from [15], in dark blue from [59], in dark green from [60], in dark magenta from [16], and in dark red from [46]. The thick blue line shows the area within $|b| \leq 2^\circ$ from the Galactic plane.

3. Results

Having obtained the LLS for all ~ 1440 accepted GRS in our search area, we ranked them in decreasing order of LLS and found ~ 210 to exceed a size of 1 Mpc. For these, overlays of radio contours on DES g, r, i -band composites were prepared and scrutinized again. As a consequence, about 30 of these were discarded for being likely separate sources, and 178 objects were accepted as new GRS, of which we mark 14 as likely candidates in Table 2 due to uncertainties in either their LAS, z_{phot} or their host ID.

As a side product, our list of smaller radio galaxies contains ~ 300 ERGs with LLS = 0.7–1.0 Mpc, plus ~ 400 with LLS = 0.5–0.7 Mpc, and 550 smaller ones. All these require further scrutinizing and will be published elsewhere. However, these numbers serve to demonstrate the significant effort necessary to find physically large sources among objects selected purely by their angular size. For example, of the 558 surviving radio galaxies with LAS $> 2.0'$, only 32% turned out to be GRS larger than 1 Mpc, and of all the 1038 with LAS $> 1.4'$, only 46% turned out to be ERGs with LLS > 0.7 Mpc. Given that from the candidates originally selected on the RACS images, about 30% had to be discarded upon closer inspection; this implies that to find a single GRS larger than 1 Mpc, one has to inspect on average 4.4 candidates larger than $2.0'$, and to find a single ERG larger than 0.7 Mpc, one has to inspect on average 3 candidates larger than $1.4'$.

3.1. The List of 178 New and 3 Known GRS in the Search Area

In what follows we shall limit ourselves to the sample of 178 new and 3 previously published GRS larger than 1 Mpc. Their sky distribution is plotted in Figure 1. In about 20 cases, the host could not be determined with certainty, and either the brightest in optical or MIR was chosen such that its redshift and linear size can be considered a lower limit. The basic properties of these 181 GRS are listed in Table 2, the columns of which are as follows: (1) name of the GRS derived from truncation of the sexagesimal equatorial J2000 coordinates of the optical host, appended with a “C” if the GRS is considered a candidate; for each object we indicate in which survey it was noticed first: P = previously published (3 objects), A = ATESP (3 objects), E = EMU Pilot Survey (8 objects), S = SUMSS (45 objects), R = RACS (122 objects); (2,3) RA and Dec (J2000) of the optical host in decimal degrees; (4) the largest angular size of the radio emission; (5) the adopted redshift and type: s for spectroscopic, p for photometric, and e for estimated, with question marks indicating uncertainty due to inconsistent z_{phot} values found (see also Section 2.4); (6) references used to select the adopted redshift: 1 [52], 2 [51], 3 [50], 4 [61], 5 [62], 6 [63], 7 [64], 8 [54], 9 [53] 10 [65], 11 [66] 12 [67], 13 [68] 14 [69]; (7) largest linear size of the radio emission; (8,9) name and type of the host object, where G = galaxy, GP = galaxy pair, GQ = galaxy or QSO, Q = QSO, Qc = QSO candidate, with a “?” sign indicating uncertainty; (10) r -band magnitude from DES; (11) integrated flux density from RACS or CRACS (see Section 2.5); (12) decimal logarithm of spectral radio power at 888 MHz; (13) position angle of the major axis of the radio source, measured from North through East; (14) radio morphology according to Table 1.

Host redshifts range from 0.02 to ~ 2.0 , but only 10 of the 178 new GRS have spectroscopic redshifts. For the 146 host galaxies, the median r -band magnitude and redshift are 20.9 and 0.64, while for the 32 QSOs or candidates, these are 19.7 and 0.75. The lowest total radio flux densities are 5.0 mJy with 10 objects fainter than 10 mJy. The lobe brightness of various GRS barely exceeds 1 mJy beam^{-1} . We compare the properties of our new sample with those of six previous large compilations of GRS in Section 4.1.

Table 2. List of 181 giant radio sources in our search area (see paper text for the description of columns). The complete table is also available at the <https://zenodo.org/record/5725939#.YZ7wdRwRVPZ>.

(1) Name, Origin	(2) RA _J (°)	(3) Dec _J (°)	(4) LAS (′)	(5) z, ztype	(6) Ref(z)	(7) LLS (Mpc)	(8) Hostname	(9) Host Type	(10) rmag (mag)	(11) S ₈₈₈ (mJy)	(12) log P ₈₈₈ (W/Hz)	(13) RPA (°)	(14) Radio Morphology		
J0004–4205	S	001.1349	−42.0852	2.95	0.53	p	1,2	1.11	DES J000432.36–420506.7	G	20.80	84.	25.93	27	FRIIrelic,ncor
J0011–4001	A	002.7774	−40.0253	2.6	0.881	s	13	1.08	HE 0008–4018	Q	17.44	30.3	26.01	59	FRIIcoredom
J0014–4542C	R	003.6338	−45.7011	4.2	0.296	p	1,3	1.11	DES J001432.11–454204.1?	G	19.53	13.4	24.55	56	FRIIremn,ncor,asym
J0016–4541	R	004.0419	−45.6857	2.2	1.07	p	1,8	1.07	DES J001610.05–454108.6	G	22.49	13.9	25.87	112	FRIIremn
J0017–4449	R	004.3794	−44.8306	2.05	1.12	p	1	1.01	DES J001731.05–444950.2	G	22.95	61.9	26.57	141	FRIIrelic
J0020–4625	R	005.0739	−46.4173	2.44	0.65	p	1,2	1.01	DES J002017.74–462502.2	G	20.66	87.4	26.16	12	FRIIremn
J0023–4732	R	005.9779	−47.5410	3.25	0.52	p	1	1.21	DES J002354.69–473227.6?	G	21.49	32.4	25.50	22	FRIIincor,naked
J0024–4816	R	006.0832	−48.2691	5.8	0.268	p	1,2	1.43	DES J002419.94–481608.5	G	18.37	34.8	24.87	50	FRIIrelic,ncor
J0024–4848	R	006.0838	−48.8115	2.37	0.90	p	1,8	1.11	DES J002420.12–484841.5	GQ	22.65	31.0	26.04	138	FRII
J0025–4946	R	006.3780	−49.7787	3.42	0.51	p	1	1.27	DES J002530.72–494643.4	G	20.70	12.9	25.08	11	FRIIcoredom
J0027–4746	S	006.7520	−47.7750	4.47	0.84	p	1	2.05	DES J002700.50–474630.0	G	21.42	211.9	26.80	149	FRII
J0029–4601	R	007.4194	−46.0246	2.79	0.50	p	1	1.02	DES J002940.66–460128.7	G	20.26	7.2	24.80	152	FRI/II,faint
J0031–4826	R	007.9993	−48.4343	3.09	0.65	p	1	1.28	DES J003159.82–482603.5	G	21.59	42.1	25.84	167	FRIIincor
J0035–4824	R	008.9547	−48.4161	2.9	0.94	p	1	1.37	DES J003549.12–482458.0	G	23.02	59.8	26.37	80	FRIIincor ?
J0036–4138	R	009.1483	−41.6435	2.55	0.57	p	1	1.00	DES J003635.58–413836.7	G	21.35	27.6	25.52	102	FRIIremn,ncor
J0038–4741C	R	009.5398	−47.6938	2.3	1.17	p	1	1.14	DES J003809.54–474137.8?	G	23.49	37.9	26.40	160	FRIIincor
J0040–4817	R	010.1491	−48.2885	7.08	0.53	p	1,2	2.67	DES J004035.77–481718.6	G	20.22	14.8	25.18	177	FRI/II
J0041–4738	R	010.3071	−47.6373	3.84	>0.4?	p	1,3,8,9	>1.24	DES J004113.71–473814.4	Qc	18.10	5.0	24.42	139	FRII
J0044–4915	S	011.1276	−49.2545	2.4	0.7?	p	1,8	1.03	DES J004430.62–491516.1	Qc	17.00	267.1	26.72	120	FRII
J0052–4238	R	013.1770	−42.6461	2.4	0.87?	p	1,8,9	1.11	DES J005242.47–423845.8	Qc	19.97	14.7	25.68	12	FRIIremn
J0052–4206	R	013.1866	−42.1058	2.14	0.92	p	1	1.01	DES J005244.79–420620.8	G	22.79	19.0	25.85	0	FRIIrelic,ncor
J0054–4825	R	013.6751	−48.4269	2.55	0.80	p	1	1.15	DES J005442.02–482536.7	G	22.26	37.7	26.00	82	FRIIremn
J0054–4952	R	013.7436	−49.8739	9.67	0.47	p	1,2	3.42	DES J005458.45–495226.0	G	19.74	24.0	25.26	156	FRII
J0103–4324	R	015.7548	−43.4082	2.8	0.874	p	1	1.30	DES J010301.15–432429.5	G	21.51	17.8	25.77	131	FRIIrelic
J0105–4505	S	016.3425	−45.0881	2.85	0.69	p	1,4	1.21	DES J010522.19–450517.2	G	20.23	4291.9	27.91	56	FRII
J0106–4602	S	016.5371	−46.0387	3.39	0.478	p	1	1.21	DES J010608.90–460219.3	G	20.20	37.0	25.47	30	FRIIincor
J0108–4843	R	017.0196	−48.7175	4.2	0.503	p	1	1.54	DES J010804.70–484302.9?	G	20.65	7.5	24.83	118	FRIIremn
J0116–4000	A	019.0221	−40.0130	3.42	1.06	p	1	1.66	DES J011605.29–400046.6	G	22.95	59.8	26.49	27	FRII
J0116–4722	P	019.1043	−47.3782	11.2	0.146	s	11	1.70	2MASX J01162507–4722406	G	15.62	4210.	26.37	169	FRII,DDRG
J0116–4555	R	019.1479	−45.9257	4.5	1.015	p	1	2.17	DES J011635.50–455532.6	Qc	23.72	15.3	25.86	132	FRIInaked
J0121–4656	R	020.3779	−46.9399	2.68	0.813	p	1	1.21	DES J012130.69–465623.6	G	22.29	39.8	26.04	27	FRIIincor
J0125–4110	R	021.4841	−41.1696	8.0	0.11852	s	7	1.03	2MASX J01255616–4110102	G	15.93	90.1	24.51	27	FRI/II,WAT?
J0126–4407	R	021.7427	−44.1182	3.9	0.364	p	1,2	1.19	DES J012658.24–440705.6	G	19.18	18.9	24.91	176	FRI/IIremn

Table 2. Cont.

(1) Name, Origin	(2) RA _J (°)	(3) Dec _J (°)	(4) LAS (′)	(5) z, ztype	(6) Ref(z)	(7) LLS (Mpc)	(8) Hostname	(9) Host Type	(10) rmag (mag)	(11) S ₈₈₈ (mJy)	(12) log P ₈₈₈ (W/Hz)	(13) RPA (°)	(14) Radio Morphology	
J0127–4610	R	021.8368	−46.1770	4.67	0.72 p	1,9	2.03	DES J012720.83–461037.0	Qc	19.78	112.2	26.37	174	FRIIasym
J0129–4330	R	022.3443	−43.5151	2.2	0.919 p	1	1.03	DES J012922.62–433054.3	G	24.32	11.3	25.62	164	FRIIncor
J0131–4901	R	022.9477	−49.0263	2.43	1.0? e	-	1.17	(DESI J022.9477–49.0263)	G	24.5?	45.4	26.32	17	FRIIremn
J0133–4655	R	023.3367	−46.9171	2.5	0.65 p	1,9	1.04	DES J013320.80–465501.4	G	20.25	38.4	25.80	10	FRIIremn
J0133–4431	R	023.4138	−44.5170	2.1	1.048 p	1	1.02	DES J013339.30–443101.1	G	22.34	274.1	27.14	6	FRII
J0135–4249	R	023.8273	−42.8276	2.64	2.0? p	8	1.33	DES J013518.56–424939.4	Qc	22.67	34.7	26.91	168	FRII
J0138–4116	R	024.6351	−41.2714	2.75?	0.954 p	1	1.31	DES J013832.41–411616.9	G	22.03	12.0	25.69	172	FRI/II,hymor?
J0138–4231	S	024.6632	−42.5272	46.	0.02123 s	5	1.19	NGC 641; ESO 244–G042	G	12.04	334.6	23.53	37	FRI/II
J0141–4759	R	025.3820	−47.9861	3.0	0.984 p	1	1.44	DES J014131.67–475909.9	G	22.10	263.6	27.06	139	FRII
J0148–4814C	R	027.2305	−48.2365	4.2	0.264 p	1,2	1.03	DES J014855.31–481411.2	G	18.44	24.0	24.69	114	FRIIremn
J0149–4036	S	027.3344	−40.6159	2.4	0.7? p	1,8,9	1.03	DES J014920.26–403657.3	Qc	19.33	46.2	25.95	35	FRI/IIremn
J0150–4507	S	027.5045	−45.1258	6.64	0.25 p	1,2	1.56	2MASX J01500108–4507331	G	17.59	105.7	25.28	10	FRII
J0150–4634	S	027.6889	−46.5833	2.48	0.88 p	1	1.15	DES J015045.33–463459.8	G	22.14	33.3	26.05	21	FRIIremn,precess?
J0205–4206	S	031.4603	−42.1121	4.6	0.31941 s	7	1.28	HE 0203–4221	Q	15.81	261.8	25.92	68	FRIIrelic
J0206–4514	R	031.5664	−45.2382	3.25	0.631 p	1	1.33	DES J020615.92–451417.3	G	20.47	61.1	25.97	55	FRIIncor
J0212–4447	R	033.1357	−44.7957	3.38	1.191 p	1	1.68	DES J021232.56–444744.4	Qc	23.69	20.6	26.15	144	FRIInaked
J0213–4744	P	033.2902	−47.7370	6.65	0.220 s	10	1.42	2MASX J02130961–4744128	G	17.35	2050.	26.45	171	FRIIplumes
J0215–4024	S	033.8490	−40.4069	3.16	0.42 p	1,2	1.05	DES J021523.75–402424.9	G	20.34	585.5	26.54	126	FRIIplumes
J0223–4826	S	035.8849	−48.4483	2.34	0.70 p	1	1.00	DES J022332.36–482654.0	G	21.03	347.3	26.83	158	FRII
J0223–4226	R	035.9365	−42.4352	4.0	>0.650 p	1	>1.66	DES J022344.76–422606.7?	G	22.60	40.2	25.82	176	FRII
J0236–4456	R	039.1024	−44.9405	3.42	0.859 p	1	1.58	DES J023624.58–445625.6	G	21.75	58.3	26.27	156	FRII
J0247–4334	S	041.8256	−43.5719	3.65	1.25 p	1,8	1.83	DES J024718.13–433418.9	GQ	22.42	52.3	26.61	26	FRII
J0252–4941	R	043.1323	−49.6991	2.85	0.664 p	1	1.20	DES J025231.75–494156.7	G	20.67	16.7	25.46	6	FRIIrelic,coredom
J0253–4806	R	043.4708	−48.1082	3.0	0.623 p	1	1.22	DES J025352.99–480629.6	G	20.37	15.9	25.37	31	FRIIrelic
J0259–4840	S	044.9775	−48.6795	3.22	0.93 p	1	1.52	DES J025954.60–484046.2	G	21.63	325.0	27.09	111	FRII
J0310–4740	S	047.5660	−47.6774	3.38	0.55 p	1	1.30	DES J031015.84–474038.5?	G	20.21	204.4	26.35	106	FRII
J0315–4443	R	048.8579	−44.7257	3.5	0.362 p	1,2	1.06	DES J031525.88–444332.4	G	19.17	21.8	24.96	106	FRII
J0320–4845	R	050.0403	−48.7665	2.67	0.645 p	1	1.11	DES J032009.68–484559.2?	Qc	23.89	25.3	25.61	88	FRIIncor
J0320–4515	P	050.2397	−45.2530	27.2	0.0633 s	6	1.99	ESO 248–G010; MSH 03@43	G	14.33	5500.	25.72	47	FRII
J0328–4208	R	052.1877	−42.1493	4.50	0.55 p	1,8,9	1.73	DES J032845.03–420857.6	Qc	18.56	39.2	25.64	35	FRIIasym
J0342–4019	S	055.6854	−40.3272	4.5	0.69 p	1	1.92	DES J034244.49–401937.7	G	20.45	382.8	26.86	107	FRII
J0344–4817	R	056.0404	−48.2896	3.36	0.380 p	1	1.05	DES J034409.70–481722.4	G	20.51	32.1	25.18	159	FRIIncor
J0346–4253	R	056.5079	−42.8945	2.75	0.604 p	1	1.11	DES J034601.89–425340.0?	G	20.66	50.8	25.84	146	FRIIrelic
J0349–4302C	R	057.3790	−43.0424	2.7	0.879 p	1	1.24	DES J034930.95–430232.4?	G	23.56	6.7	25.35	31	FRIIncor

Table 2. Cont.

(1) Name, Origin	(2) RA _J (°)	(3) Dec _J (°)	(4) LAS (′)	(5) z, ztype	(6) Ref(z)	(7) LLS (Mpc)	(8) Hostname	(9) Host Type	(10) rmag (mag)	(11) S ₈₈₈ (mJy)	(12) log P ₈₈₈ (W/Hz)	(13) RPA (°)	(14) Radio Morphology		
J0352–4626	R	058.0616	−46.4406	2.8	0.591	p	1	1.12	DES J035214.77–462626.1	G	20.89	125.7	26.22	82	FRIIrelic
J0352–4756	R	058.1879	−47.9477	2.7	0.927	p	1	1.27	DES J035245.09–475651.8	G	21.50	9.7	25.57	135	FRIIrelic
J0352–4536	R	058.2474	−45.6046	2.4	0.65	p	1	1.00	DES J035259.37–453616.6	G	21.59	87.3	26.16	14	FRIIrelic,asym
J0353–4446	R	058.3342	−44.7831	3.55	0.353	s	13	1.06	HE 0351–4455	Q	16.69	367.3	26.16	87	FRIIbent
J0354–4728	R	058.5263	−47.4737	2.95	1.021	p	1	1.42	DES J035406.30–472825.1	G	22.90	90.0	26.63	60	FRIIncor
J0355–4258C	R	058.7883	−42.9702	2.28	0.81	p	1	1.03	DES J035509.18–425812.7?	G	22.19	48.1	26.12	119	FRIIrelic
J0356–4503	S	059.1046	−45.0665	2.1	1.13	p	1	1.03	DES J035625.11–450359.2	G	24.12	69.9	26.63	80	FRII
J0359–4800	R	059.8806	−48.0059	2.9	0.679	p	1	1.23	DES J035931.34–480021.3	G	20.73	28.2	25.71	10	FRII
J0406–4544	S	061.5326	−45.7476	6.4	0.315	p	1,2	1.77	DES J040607.82–454451.2	G	18.26	77.0	25.37	131	FRII
J0406–4429	S	061.7500	−44.4945	11.8	0.1408	s	7	1.76	2MASX J04065999–4429400	G	15.60	18.1	23.97	105	FRI/IIremn
J0407–4538	R	061.8515	−45.6480	2.23	0.903	p	1	1.04	DES J040724.34–453852.8?	G	22.40	32.6	26.07	28	FRIIrelic
J0410–4012	R	062.5550	−40.2104	2.33	0.91	p	1	1.09	DES J041013.20–401237.4?	G	22.41	34.8	26.10	31	FRIIbent
J0412–4819C	S	063.1106	−48.3220	4.3	>0.26	p	1	>1.04	DES J041226.53–481919.2	GP	19.63	45.0	24.95	89	FRIIncor ?
J0420–4509	S	065.2422	−45.1645	7.2	0.32	p	1,2,9	2.00	DES J042058.13–450952.0	G	19.04	440.6	26.14	133	FRIIplume
J0422–4518C	R	065.5653	−45.3096	>7.5?	0.388	p	1,2	2.37	DES J042215.67–451834.6	G	19.69	69.0	25.53	61	FRI
J0425–4340C	R	066.2899	−43.6825	2.38	0.895	p	1	1.11	DES J042509.56–434056.8	G	21.62	86.2	26.48	144	FRII
J0425–4823	S	066.3343	−48.3871	2.46	0.86	p	1,8	1.13	DES J042520.22–482313.5	GQ	21.09	137.0	26.64	129	FRII
J0429–4517	S	067.3708	−45.2908	5.0	0.545	p	1,2	1.91	DES J042928.98–451726.7	G	19.74	195.5	26.33	15	FRIIrelic
J0431–4823	R	067.9135	−48.3954	2.76	0.704	p	1	1.19	DES J043139.24–482343.3	G	21.71	51.9	26.01	122	FRII
J0433–4948	R	068.3529	−49.8026	2.51	0.592	p	1	1.00	DES J043324.68–494809.2?	G	21.46	27.2	25.55	35	FRI/IIcoredom,hymor?
J0433–4022	R	068.3570	−40.3824	2.85	0.555	p	1	1.10	DES J043325.68–402256.7	G	21.14	20.4	25.36	7	FRIIrelic
J0440–4742	R	070.1712	−47.7097	6.63	0.302	p	1,2	1.78	DES J044041.09–474234.9	G	18.56	36.3	25.00	52	FRIIremn
J0442–4716	R	070.5712	−47.2812	3.4	0.356	p	1,2	1.02	DES J044217.08–471652.4	G	18.35	8.2	24.52	72	FRIIrelic
J0448–4151	S	072.2195	−41.8611	4.08	0.694	p	1	1.74	DES J044852.67–415140.0	G	21.45	93.8	26.25	174	FRII
J0449–4022	S	072.2808	−40.3793	2.2	0.9?	p	1,8,9	1.03	DES J044907.38–402245.4	Qc	19.65	35.5	26.10	159	FRII
J0450–4722	S	072.5735	−47.3736	2.35	1.5	p	8,9	1.19	DES J045017.64–472225.1	Qc	17.23	597.9	27.85	45	FRII
J0452–4040	S	073.2427	−40.6699	4.05	0.33	p	1,2	1.15	DES J045258.25–404011.5	G	18.84	102.6	25.54	8	FRIIncor
J0457–4137	R	074.2901	−41.6327	2.76	0.596	p	1	1.10	DES J045709.61–413757.6	G	21.07	21.3	25.45	35	FRIIncor
J0457–4445	R	074.4563	−44.7635	3.55	0.581	p	1,2	1.40	DES J045749.50–444548.4	G	20.69	24.1	25.48	125	FRIIasym
J0458–4659	S	074.5083	−46.9964	3.25	0.45	p	1,2	1.12	DES J045801.98–465947.1	G	19.95	626.3	26.64	118	FRIIrelic
J0459–4637	R	074.8534	−46.6192	6.43	0.310	p	1,2	1.76	DES J045924.80–463709.1	G	18.20	30.0	24.95	171	FRIIrelic
J0459–4507	S	074.9130	−45.1326	2.45	0.62	p	1	1.00	DES J045939.12–450757.3	G	20.75	74.7	26.04	23	FRII
J0500–4242	R	075.0310	−42.7108	5.88	1.1	p	1,8,9	2.88	DES J050007.44–424238.7	Qc	18.87	25.0	26.15	73	FRIInaked
J0502–4723C	R	075.6359	−47.3996	2.75	0.94	p	1	1.30	DES J050232.61–472358.4?	G	23.44	12.5	25.69	72	FRII

Table 2. Cont.

(1) Name, Origin	(2) RA _J (°)	(3) Dec _J (°)	(4) LAS (′)	(5) z, ztype	(6) Ref(z)	(7) LLS (Mpc)	(8) Hostname	(9) Host Type	(10) rmag (mag)	(11) S ₈₈₈ (mJy)	(12) log P ₈₈₈ (W/Hz)	(13) RPA (°)	(14) Radio Morphology		
J0507–4248	S	076.9394	−42.8065	3.7	0.46	p	1,8	1.29	DES J050745.45–424823.3	Qc	18.76	73.1	25.73	81	FRII
J0508–4737C	R	077.0647	−47.6263	6.54	0.421	p	1,2	2.17	DES J050815.53–473734.5	G	18.94	60.5	25.55	35	FRII
J0509–4619	R	077.3847	−46.3188	2.74	0.66	p	1	1.15	DES J050932.33–461907.6	G	21.22	39.1	25.82	107	FRII
J0519–4654	S	079.7541	−46.9148	3.8	0.5?	p	1	1.39	DES J051900.97–465453.3?	G	21.48	114.2	26.00	123	FRII
J0524–4235C	R	081.0285	−42.5939	6.16	>0.65?	p	1,8	>2.56	DES J052406.82–423537.9	Qc	19.89	42.1	25.84	166	FRII?
J0524–4903	R	081.1285	−49.0535	2.28	1.14	p	1	1.12	DES J052430.84–490312.5	Qc	23.88	25.8	26.20	42	FRII?
J0528–4057	R	082.1046	−40.9601	2.4	0.9?	p	1,8	1.12	DES J052825.10–405736.3	Qc	23.24	32.9	26.07	167	FRII
J0532–4118	R	083.2079	−41.3158	2.74	0.72	p	1	1.19	DES J053249.90–411856.8	G	20.94	22.1	25.66	44	FRII,WAT?
J0533–4907	S	083.4639	−49.1298	3.25	0.50	p	1,2	1.19	DES J053351.34–490747.3	G	19.93	85.7	25.88	38	FRIIasym
J0533–4312	R	083.4847	−43.2054	4.15	0.70	p	1	1.78	DES J053356.31–431219.5	G	21.33	36.4	25.85	102	FRIIncor
J0545–4350	R	086.4777	−43.8415	4.88	0.64	p	1	2.01	DES J054554.64–435029.2	G	20.47	41.8	25.82	59	FRIIncor
J0550–4014	R	087.6864	−40.2486	3.1	0.9?	p	1,8	1.45	DES J055044.73–401455.1	Qc	21.65	48.0	26.23	40	FRIIrelic
J0551–4519	R	087.7760	−45.3332	2.3	1.07	p	1	1.12	DES J055106.24–451959.6	G	22.59	59.3	26.50	81	FRII
J0551–4902	R	087.9728	−49.0364	3.0	1.31	p	1	1.51	DES J055153.46–490211.0	G	24.25	10.3	25.95	50	FRII
J0554–4103	S	088.6400	−41.0624	3.00	0.87	p	1	1.39	DES J055433.59–410344.5	G	22.34	162.5	26.73	109	FRII
J0600–4908	R	090.1793	−49.1469	3.55	1.2	p	1	1.77	DESI J090.1793–49.1469 ?	G?	23.49	61.2	26.63	79	FRIIasym ?
J0604–4459	R	091.1750	−44.9970	3.07	0.78	p	1	1.37	DES J060441.98–445949.1	G	22.29	72.6	26.26	158	FRII
J0609–4518	R	092.3167	−45.3051	5.99	0.513	p	1	2.22	DES J060915.99–451818.2	G	19.37	52.0	25.69	2	FRII
J0618–4628	S	094.7272	−46.4721	7.32	0.39	p	1,2	2.32	DES J061854.52–462819.3	G	19.57	252.3	26.10	9	FRII
J2022–4156	R	305.5250	−41.9452	2.52	0.800	p	1	1.14	DES J202206.00–415642.8	Qc	21.31	40.5	26.03	74	FRII
J2022–4618	R	305.5850	−46.3011	3.6	0.35?	p	1,2	1.06	DES J202220.40–461803.8?	Qc	20.00	33.7	25.12	14	FRIIncor,asym
J2024–4947	R	306.2337	−49.8000	2.65	0.86	p	1	1.22	DES J202456.08–494759.8?	G	21.77	17.9	25.75	174	FRIIrelic,ncor
J2025–4003	R	306.2775	−40.0619	6.0	0.57	p	1	2.35	DES J202506.58–400342.8	G	21.08	185.2	26.35	10	FRII
J2029–4119	S	307.4041	−41.3174	4.0	0.355	p	1,2	1.20	DES J202936.98–411902.7	G	18.45	1350.	26.73	148	FRII
J2041–4546	R	310.3727	−45.7767	2.8	0.82	p	1	1.27	DES J204129.45–454636.2	G	20.91	100.2	26.45	22	FRII
J2042–4801	R	310.5939	−48.0302	2.2	0.83	p	1	1.00	DES J204222.52–480148.8	G	21.75	43.2	26.10	60	FRIIrelic
J2045–4340	R	311.2527	−43.6793	3.5	0.978	p	1	1.67	DES J204500.64–434045.5	G	23.33	135.3	26.77	66	FRIIrelic
J2049–4014	R	312.2829	−40.2416	3.8	0.475	p	1,2	1.35	DES J204907.89–401429.7	G	20.01	10.9	24.93	125	FRIIrelic
J2050–4647	S	312.5283	−46.7885	4.91	0.55	p	1,2	1.89	DES J205006.79–464718.5	G	20.76	74.9	25.92	0	FRII
J2052–4813	E	313.0764	−48.2225	4.91	0.395	p	1,2	1.57	DES J205218.33–481321.2	G?	19.71	55.4	25.45	77	FRII
J2054–4431	R	313.7169	−44.5245	3.0	0.55	p	1	1.16	DES J205452.05–443128.3	G	20.50	12.1	25.13	34	FRIIrelic
J2055–4413C	R	313.8971	−44.2268	3.1	0.399	p	1,2	1.00	DES J205535.29–441336.5	G	19.25	6.3	24.52	179	FRIIrelic
J2056–4821	E	314.0627	−48.3567	7.0	0.35	p	1,2,8	2.07	DES J205615.04–482123.9	G	19.14	10.2	24.60	98	FRII
J2056–4845	E	314.2441	−48.7567	2.35	0.94	p	1	1.11	DES J205658.59–484524.4	G	22.43	21.3	25.92	21	FRII

Table 2. Cont.

(1) Name, Origin	(2) RA _J (°)	(3) Dec _J (°)	(4) LAS (′)	(5) z, ztype	(6) Ref(z)	(7) LLS (Mpc)	(8) Hostname	(9) Host Type	(10) rmag (mag)	(11) S ₈₈₈ (mJy)	(12) log P ₈₈₈ (W/Hz)	(13) RPA (°)	(14) Radio Morphology		
J2108–4336	R	317.1310	−43.6134	2.95	1.06	p	1	1.44	DES J210831.43–433648.3	G	22.06	124.6	26.81	84	FRII
J2110–4112	R	317.5495	−41.2031	3.9	0.392	p	1,2	1.24	DES J211011.87–411211.1	G	18.50	56.1	25.45	0	FRIIbent,WAT?
J2111–4948	E	317.9387	−49.8122	4.49	0.283	p	1,2	1.15	DES J211145.28–494843.9	G	18.70	24.3	24.77	32	FRII
J2117–4415	R	319.3348	−44.2578	3.2	0.7?	p	1,2,8,9	1.37	DES J211720.35–441528.1	Qc	19.34	66.3	26.11	23	FRII
J2138–4435C	R	324.6969	−44.5844	4.39	1.06	p	1	2.14	DES J213847.26–443503.7	G	22.52	13.0	25.83	114	FRII
J2144–4818	E	326.0088	−48.3159	7.95	0.136	p	1,2	1.15	2MASX J21440210–4818581	G	17.03	191.2	24.96	167	FRIIremn,ncor
J2149–4226	R	327.3891	−42.4441	2.63	0.66	p	1,2,8,9	1.12	DES J214933.38–422638.7	GQ	19.56	402.0	26.83	163	FRII
J2152–4911	E	328.1957	−49.1952	2.95	0.58	p	1,2	1.16	DES J215246.97–491142.9?	G	20.05	30.7	25.58	102	FRII
J2154–4552	S	328.5959	−45.8753	7.2	0.1453	s	7	1.10	2MASX J21542297–4552315	G	16.12	1106.	25.79	40	FRIIasym
J2155–4235	S	328.8819	−42.5867	3.47	>0.70	p	8,9,14	>1.49	DES J215531.65–423512.0	Qc	18.46	132.5	26.41	38	FRII
J2202–4004	R	330.6272	−40.0686	5.1	0.86	p	1	2.35	DES J220230.53–400406.8?	G	21.62	39.1	26.09	166	FRII
J2205–4810	R	331.4580	−48.1686	2.65	0.60	p	1	1.06	DES J220549.91–481007.0	GP	21.47	16.3	25.34	161	FRIIrelic
J2215–4225	R	333.8671	−42.4300	3.5	0.42	p	1	1.16	DES J221528.11–422548.0	G	18.75	8.1	24.68	22	FRIIremn
J2216–4328	R	334.2185	−43.4674	2.05	1.6?	p	1,8	1.04	DES J221652.36–432802.2?	Qc	24.60	5.0	25.84	164	FRII
J2218–4959	E	334.5944	−49.9908	2.4	0.8?	p	1	1.03	DES J221822.66–495927.0	G	24.35	10.0	25.43	78	FRII
J2219–4748	R	334.7847	−47.8047	3.1	0.46	p	1,2	1.08	DES J221908.32–474816.8	Qc	18.78	10.3	24.88	172	FRIIrelic
J2220–4854	E	335.1798	−48.9048	2.53	0.80	p	1	1.14	DES J222043.14–485417.1	G	20.42	16.1	25.64	125	FRII
J2224–4724	S	336.0727	−47.4009	3.7	0.85	p	1	1.70	DES J222417.45–472403.2	G	22.66	96.7	26.48	85	FRII
J2226–4316	R	336.6399	−43.2765	13.8	0.09309	s	12	1.43	2MASX J22263358–4316356	G	17.75	170.	24.56	153	FRIIremn
J2226–4624C	R	336.7430	−46.4036	2.62	1.40	p	1	1.33	DES J222658.31–462413.1	Qc	23.88	44.9	26.66	11	FRIIncor
J2228–4210	S	337.0102	−42.1740	4.94	0.55?	p	1,2	1.90	DES J222802.44–421026.4	G	20.51	93.8	26.02	171	FRII
J2232–4025	R	338.1574	−40.4270	3.78	0.68	p	1	1.60	DES J223237.77–402537.2	G	21.21	12.8	25.37	25	FRIIrelic
J2236–4113	R	339.2012	−41.2225	4.56	0.3	p	1,2,9	1.22	DES J223648.28–411321.0	G	19.12	61.0	25.22	13	FRII
J2239–4450	S	339.8511	−44.8384	3.4	0.42	p	1	1.13	DES J223924.27–445018.1	G	19.84	34.8	25.31	156	FRII
J2240–4724	S	340.1112	−47.4028	12.	0.09161	s	7	1.23	2MASX J22402674–4724100	G	15.41	53.	24.04	25	FRIIremn,DDRG?
J2245–4239	R	341.4210	−42.6533	2.54	1.00	p	1	1.22	DES J224541.03–423911.8	G	21.48	15.5	25.85	7	FRII
J2246–4934	R	341.7351	−49.5830	3.4	0.80	p	1	1.53	DES J224656.42–493458.9	G	21.87	27.7	25.87	170	FRII
J2247–4034	A	341.7816	−40.5705	2.75	0.53	p	1,8,9,14	1.04	DES J224707.59–403413.7	Qc	19.72	64.5	25.82	16	FRII
J2247–4753	R	341.9390	−47.8977	3.6	0.34	p	1	1.05	DES J224745.37–475351.8	G	21.69	7.0	24.41	30	FRII
J2250–4751	S	342.6531	−47.8643	4.04	0.32	p	1,2	1.13	DES J225036.75–475151.5	G	18.84	22.6	24.85	121	FRII
J2253–4424	R	343.2764	−44.4038	2.53	1.07	p	1	1.23	DES J225306.34–442413.6?	G	22.25	63.1	26.53	175	FRIIncor
J2258–4819	R	344.5067	−48.3254	3.0	0.98	p	1	1.43	DES J225801.59–481931.2	G	22.99	17.3	25.87	63	FRII
J2301–4359	R	345.4059	−43.9971	8.0	0.11685	s	7	1.01	2MASX J23013741–4359497	G	15.33	160.6	24.75	7	FRI/Irelic,precess
J2306–4045	S	346.6868	−40.7622	5.24	0.28	p	1,2	1.33	DES J230644.84–404543.9	G	19.31	46.9	25.04	94	FRIIremn,ncor

Table 2. Cont.

(1) Name, Origin	(2) RA _J (°)	(3) Dec _J (°)	(4) LAS (′)	(5) z, ztype	(6) Ref(z)	(7) LLS (Mpc)	(8) Hostname	(9) Host Type	(10) rmag (mag)	(11) S ₈₈₈ (mJy)	(12) log P ₈₈₈ (W/Hz)	(13) RPA (°)	(14) Radio Morphology		
J2307–4049	R	346.8101	−40.8251	3.3	0.71	p	1	1.42	DES J230714.42–404930.5	G	21.66	16.0	25.51	179	FRII
J2317–4645	R	349.3573	−46.7614	2.7	0.80	p	1	1.22	DES J231725.76–464540.8	Qc	20.40	23.2	25.79	55	FRII
J2319–4449	R	349.8362	−44.8181	2.8	0.76	p	1	1.24	DES J231920.68–444905.1	G	20.94	33.5	25.90	22	FRII
J2325–4311	R	351.2995	−43.1922	4.48	1.03	p	1	2.17	DES J232511.86–431131.9	G	22.82	42.2	26.31	85	FRII
J2325–4153	R	351.3907	−41.8939	3.0	0.51	p	1	1.11	DES J232533.76–415338.0	G	20.22	21.6	25.30	122	FRIIremn,ncor
J2331–4928	R	352.9503	−49.4797	2.44	1.24	p	1	1.22	DESI J352.9504–49.4797	G	24.05	66.2	26.70	49	FRIIrelic
J2345–4754	R	356.3691	−47.9028	2.5	0.74	p	1	1.09	DES J234528.57–475410.1	G	21.27	15.1	25.53	165	FRI/II
J2345–4642	R	356.4543	−46.7158	4.2	0.56	p	1	1.63	DES J234549.04–464256.8	G	19.98	76.6	25.95	67	FRIIncor
J2347–4047	R	356.9115	−40.7904	4.0	0.50	p	1	1.46	DES J234738.75–404725.5	Qc	22.61	12.7	25.05	156	FRII
J2347–4837	R	356.9846	−48.6326	2.48	1.35	p	1,8,9	1.25	DES J234756.29–483757.3	Qc	18.13	21.3	26.30	139	FRIIrelic
J2350–4232	S	357.5374	−42.5375	2.6	0.99	p	1	1.25	DES J235008.98–423215.1	G	22.59	25.1	26.05	167	FRIIrelic
J2357–4010	R	359.3201	−40.1831	3.55	0.50	p	1	1.29	DES J235716.83–401059.0	G	20.34	48.7	25.64	81	FRIIrelic

3.2. The Variety of Source Morphologies, Sizes, and Radio Luminosities

Within the classification scheme we used (see Table 1), we find that the vast majority of the newly found GRS are FR II (166 or 93%), of which 30 did not have a radio core detected (i.e. $S_{888,core} \lesssim 0.5$ mJy), four have virtually unresolved lobes (tagged as “naked” in Table 1), and one (J0023–4732) shares both of the latter properties. Apart from these clear FR IIs, we found 11 (6.2%) mixed types I/II, and only a single one (J0422–4518C) is of type FR I and classified as a candidate WAT with very bent, diffuse, and low surface brightness lobes. We tagged 21 of the GRS as “remnant” and 34 as “relic” sources, which refers to the degree of diffuseness of the lobes. These will be discussed in Section 3.2.4. Since we use the tag “relic” only in connection with the tag FR II, there should not be any confusion with “relic” radio sources found in clusters of galaxies and not associated with individual host galaxies. Nine FR IIs were labeled as “asymmetric”, implying that the most likely host was found more than ~ 2 times closer to one of the outer lobes than the other. This is not unusual given that the ratio of the larger to smaller distance of hotspots of FR IIs to their host can reach and exceed five [41]. Apart from the known double–double GRS (J0116–4722), only one other noteworthy example (J2240–4724) of this type of source was found. No clear examples of hybrid morphology sources (see e.g., [70]) were found except for possibly J0138–4116 and J0433–4948, and no single example of the so-called “Odd radio circles” (ORC [71]) was found in our inspection of RACS.

While the original FR classification [40] suggested a clear-cut separation of these types in radio luminosity, it was later shown that the dividing radio luminosity not only increases with optical luminosity [72,73] but also that there is a large overlap in radio luminosities between these types (e.g., [74,75]). In our new sample of GRS, we can see only a marginal trend in the median $\log P_{888}$ from 25.0 for the 12 FR I or FR I/II sources, 25.7 for the 51 FR II relic or remnant sources, and 26.0 for the 76 clear FR II sources. We defer any discussion of this so-called “Radio-HR” [76] or Owen–Ledlow diagram [73] to a later paper, including smaller sources with a more appreciable fraction of FR I types.

As noted in Section 2.5, our algorithm for flux integration includes an estimate of equipartition parameters, assuming $k = 1$ for the proton-to-electron energy ratio, a filling factor of 1, a uniform source magnetic field in the plane of the sky, and $\alpha = -0.8$ for the source’s spectral index [57]. For the source lobes, excluding the core emission, we find magnetic fields, B_{eq} , of ~ 0.9 – 3.0 μG (0.09 – 0.3 nT) independent of using RACS or CRACS, and minimum energy densities in particles and fields, u_{min} , of ~ 1.4 – 17×10^{-14} J m^{-3} for RACS, and 0.8 – 14×10^{-14} J m^{-3} for CRACS. The minimum total energies range from 1.4×10^{50} J to 1.7×10^{54} J for RACS and from 2×10^{50} J to 2.2×10^{54} J for CRACS. The median values are comparable to those found for 3C 236 by [1]. We defer a more detailed discussion of this to a later paper.

In what follows, we select a few examples of the variety of GRS we found by means of overlays of CRACS contours on g, r, i -band composites from DES DR1. We recommend viewing these images at an amplified scale to appreciate the optical host and its environment in more detail.

3.2.1. Radio Sources Exceeding an LLS of 2 Mpc

The previously published compilations of 458 GRS (see Section 4.1) comprise six GRS (1.3%) with LLS > 3 Mpc and 52 (11.4%) larger than 2 Mpc. We find similar fractions in our sample of 178 new GRS: there is one GRS (0.6%) larger than 3 Mpc and 18 (10%) larger than 2 Mpc. Our largest GRS is J0054–4952, hosted by the $r = 19.4$ mag galaxy DES J005458.45–495226.0 at $z_{phot} = 0.47$ (based on values of 0.46 and 0.49 from [51,52]), giving an LLS of 3.4 Mpc. The second largest is J0500–4242, hosted by the $r = 18.9$ mag QSO candidate DES J050007.44–424238.7 at $z_{phot} = 1.1$ (based on values of 0.85, 1.1, and 1.5 from [52–54]), giving an LLS of 2.9 Mpc. In the six literature compilations (Section 4.1), there is only one GRS with both $z > 1$ and LLS > 2 Mpc, the QSO FBQS J0204–0944 at $z_{spec} = 1.004$ with LLS = 2.1 Mpc, making our new find of J0500–4242 the largest GRQ known at $z > 1$. We classify the latter as “FR II naked”, since the outer lobes are barely

resolved with little or no indication of a radio tail or bridge pointing towards the host. Future higher-resolution and sensitivity radio observations should show some extended structure around these hotspots. Both these GRS are shown in Figure 2.

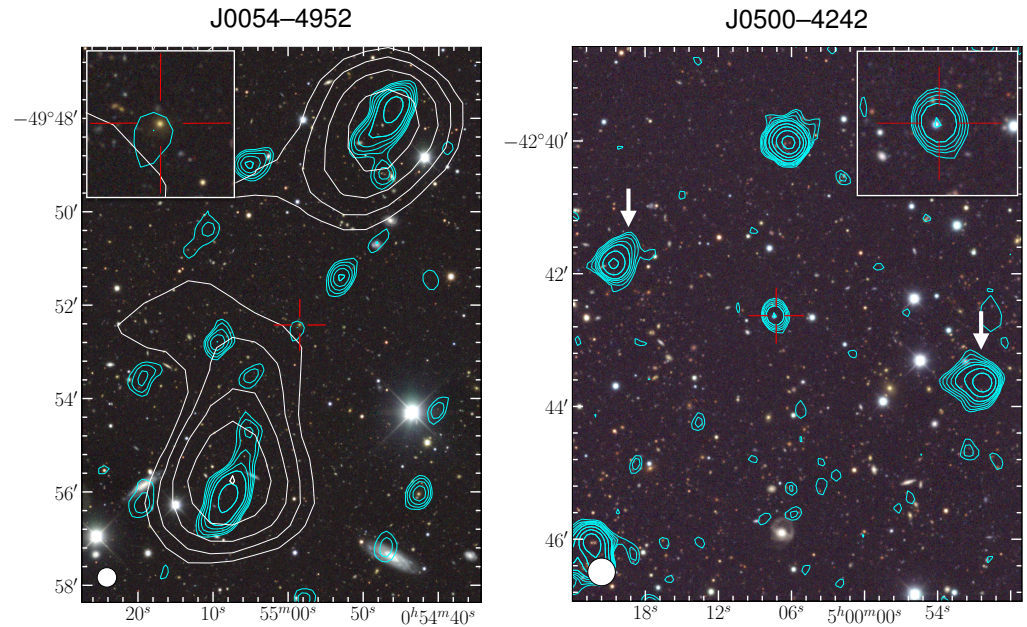


Figure 2. The two largest GRS in our sample: the GRG J0054–4952 of 3.4 Mpc (**left**) and the GRQ J0500–4242 of 2.9 Mpc (**right**), overlaid on a g, r, i composite of optical images from DES DR1. Green contours from CRACS are plotted at $2 \times [1, 2^{1/2}, 2^1, 2^{3/2}, 2^2, \dots] \times \text{rms}$. The gapped red crosses at the center mark the location of the hosts. The insets show a zoom of an area of $1' \times 1'$ around the hosts. The left panel shows additional contours from GLEAM [77] in the 170–231 MHz band, plotted at the same contour intervals, but with $\text{rms} = 6 \text{ mJy beam}^{-1}$ for a beam size of $\sim 2'$. These delineate the outer lobes, while in the right panel the lobes are indicated with white arrows.

3.2.2. Asymmetric Sources and Wide-Angle Tails (WATs)

About nine of our newly found GRS have ratios of their opposite lobe lengths of about two. The left panel of Figure 3 shows the example of J0457–4445 hosted by the $r = 20.7$ mag galaxy DES J045749.50–444548.4 at $z_{\text{phot}} = 0.58$, giving an LLS of 1.4 Mpc.

WATs tend to occur exclusively in clusters of galaxies and are predominantly hosted by the brightest cluster member. Although they are generally considered of FRI type, they appear as either jet-dominated FRI types or lobe-dominated FR II types or a mixture thereof. There are no clear-cut examples of giant WATs in our sample, and the object that comes closest to this morphology is J0532–4118 at $z_{\text{phot}} = 0.72$, with LLS ~ 1.2 Mpc, hosted by the $r = 20.9$ mag galaxy DES J053249.90–411856.8 (right panel of Figure 3). The DES image shows indications of a distant cluster, in fact, listed as ID 4063500118 by [78] and as WaZP DES YR1 J053249.9–411856 in [79], with the GRG host being the brightest member in the i -band and the third-brightest in the r -band (the brightest in r is located $33''$ N of the WAT host). WAT-type sources are not expected to grow to sizes larger than about a Mpc, since they tend to be located near the density peak of the intracluster medium of their host cluster. Thus, J0532–4118 may be exceptional, also for its high redshift. It is difficult to identify the largest WAT reported in the literature, given that this morphological type is rarely mentioned in publications on GRS, but, e.g., J2233 + 1315 hosted by the $r = 15.2$ mag, $z_{\text{phot}} = 0.093$ galaxy 2MASX J22330133+1315019, which is the brightest of cluster WHL J223301.3+131503 extends over $14.7'$ or ~ 1.7 Mpc [80]¹, or else the FRI source J1049+5513 listed in [84] and hosted by 2MASX J10490732+5513153 at $z_{\text{spec}} = 0.1262$ can be seen to extend over $11.5'$ or 1.56 Mpc in the Lockman Hole LoTSS Deep Field [85]. Since the radio morphology of the latter is quite likely foreshortened by projection, surveys such

as LoTSS or EMU should reveal even larger WATs that are oriented closer to the plane of the sky.

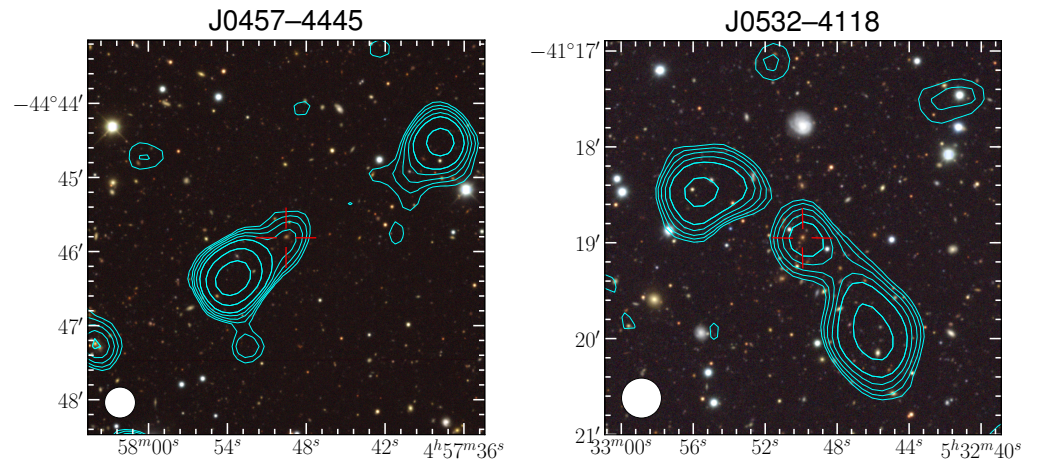


Figure 3. (Left): an example of an asymmetric GRS J0457–4445 of size 1.4 Mpc; (Right): the WAT-type source J0532–4118 in a $z \sim 0.7$ cluster. Background image, contour levels, and gapped red cross are as in Figure 2.

3.2.3. Giant Radio Sources associated with Clusters of Galaxies

Although the visual classification of the environment of the GRS hosts in our sample is beyond the scope of this work, we cross-matched the 181 GRS of Table 2 with major cluster catalogs and found the following coincidences.

The host galaxy of J0406–4544 is the brightest and dominant member of cluster WHY J040607.9–454451 at $z_{phot} = 0.315$ [86]. The radio source is a symmetric and straight FR II of projected size 1.8 Mpc, with its radio axis oriented perpendicular to the optical major axis of the outer halo of the host galaxy, but $\sim 25^\circ$ off from perpendicular for the innermost isophotes, suggesting the presence of isophote twist. The cluster is rather poor and scattered and as yet unreported as X-ray emitter.

A cross-match of our 181 GRG hosts with 2.52 million member galaxies of 60,542 clusters of the WaZP cluster catalog [79] yielded 14 matches, of which two are unlikely cluster members, seven are brightest members (one is the above-mentioned J0532–4118), and another five are lower-ranked members. The six other brightest cluster members (J0020–4625, J0105–4505, J0213–4744, J0429–4517, J0508–4737, and J2250–4751) are all hosts of fairly straight FR II-type GRS, which is considered rare. All five lower-ranked cluster member GRS hosts are also FR IIs, and special mention is deserved for the GRS J0150–4507, which is the second-brightest member of the very rich and filamentary cluster WaZP DES YR1 J015035.3–451112 at $z_{phot} \sim 0.3$, also detected via the Syunyaev–Zeldovich (SZ) effect as PSZ2 G273.69–68.38 and SPT-CL J0150–4511. The GRS host lies in a filament $\sim 7'$ (~ 1.9 Mpc) NW of the cluster center, with its radio source axis oriented perpendicular to the galaxy filament, similar to the trend seen by [26,27].

In a cross-match of our 181 GRG hosts with 12.0 million member galaxies of 540,432 clusters from the DESI Legacy Imaging Surveys [78], we found seven more GRS that are brightest cluster members, namely J0406–4429, J2052–4813, J2226–4316, J2240–4724, J2301–4359, and J2325–4153, and four more lower-ranked cluster members.

In conclusion, we find 13 of 181 GRGs ($\sim 7\%$) to be the brightest cluster members, and 9 ($\sim 5\%$) are lower-ranked members, of which J0320–4515 have already been reported as members of Abell S0345. Similar fractions of GRS in clusters were reported by [15,59].

3.2.4. Remnant Radio Sources

There is as yet no consensus about the criteria to classify radio galaxies as of the “remnant” type [87–89], especially about whether to consider the presence of a radio core.

Here we have made a crude attempt to assign the tag “remnant” to objects with very diffuse and little-collimated lobes, and “relic” to objects with moderate indications of the latter, suggesting the absence, or at least relative faintness, of any hotspots in these lobes. Note that these tags were given as a proxy for the suspected age of the lobes, *independently* of the presence of a radio core, because (a) the presence of a radio core does not seem to have any relation with the age of the lobes and (b) it could be an indication of restarting activity after a previous cycle of “feeding” a pair of lobes with relativistic particles. Thus the absence of a radio core is by no means an indicator of the final “death” of the radio activity. Figure 4 shows two examples: at left is J0133–4655, hosted by the $r = 20.3$ mag galaxy DES J013320.80–465501.4 at $z_{phot} = 0.65$ with LLS = 1.04 Mpc. The galaxy near the center of the South (S) lobe is barely detected in WISE and is considered a chance superposition. The fact that the S lobe is closer to the host and ~ 1.4 times more luminous than the North lobe, which is consistent with statistical expectation [41]. On the right is J0150–4634 (DES J015045.33–463459.8) at $z_{phot} = 0.88$, of 1.15 Mpc. The extended emission near the host is oriented at an angle of $\sim 30^\circ$ from the axis connecting the outer lobes, suggesting the central engine is both precessing, as well as restarting its radio activity.

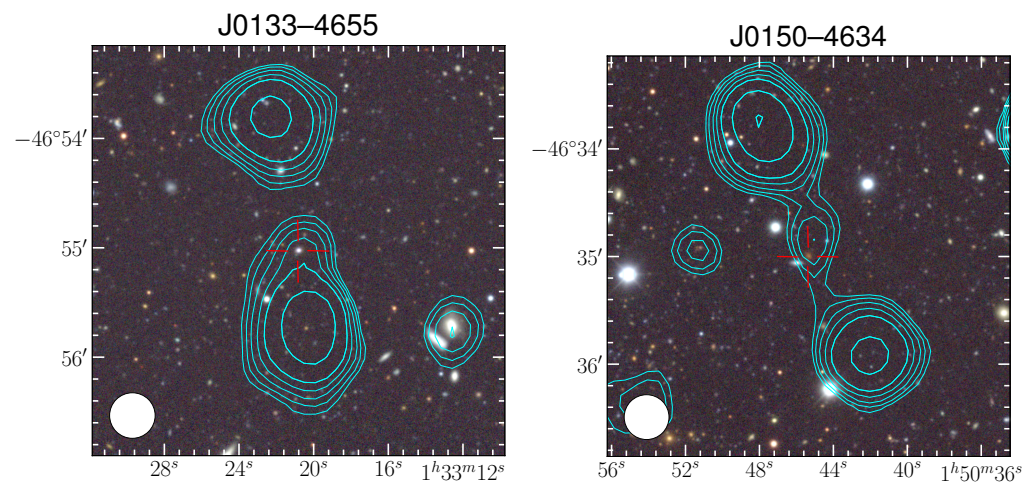


Figure 4. Two examples of remnant-type GRS. On the (left) is J0133–4655 of size 1.0 Mpc, and on the (right) J0150–4634 of size 1.2 Mpc with indications of precession. Background image, contour levels, and gapped red cross are as in Figure 2.

4. Discussion

The three previously reported GRS in our search area are J0320–4515 of 1.8 Mpc [90], and J0116–4722 and J0213–4744 of 1.8 and 1.3 Mpc, respectively, published by [91]. Their redshifts range from 0.063 to 0.146 and their total 843-MHz flux densities from SUMSS range from 2.1 to 6.7 Jy. Our new sample of GRS at high galactic latitude ($|b| \gtrsim 25^\circ$) between Dec -40° and -50° has hosts in the redshift range from 0.021 to ~ 2.0 with total 888-MHz flux densities as low as 5.0 mJy and a median of ~ 40 mJy.

4.1. Comparison of Our Sample with Previously Published GRS

The literature compilation of GRGs by [5] contains 223 objects larger than 1 Mpc, and after that, four further large samples of GRGs and one of GRQs were published. These contain (after correction of their LAS measures and exclusion of a few spurious objects consisting of separate sources) 68, 48, 18, and 25 GRS from [15,16,59,60] and 76 GRQs from [46]. This makes a total of 458 GRS published, neglecting here a few others that were reported in much smaller numbers in various papers, sometimes not even mentioning their GRS nature. Our new list of 178 GRS thus not only increases this number by $\sim 39\%$ from 458 to 636 but is also the largest yet published individual list of newly found GRS.

Table 3 compares the six published samples (first six rows) with our new sample (last row). Columns are (1) the surveys used and reference, (2) their frequency of observation,

(3) the number of GRS >1 Mpc published, (4) the median LAS, (5) lowest and median total flux density of the GRS, (6) lowest and median decimal logarithm of the radio spectral power at the frequency listed in col. 2, (7) median redshift of the hosts, (8) the fraction of hosts with spectroscopic redshift, and the fraction of hosts that are QSOs or candidates, and (9) the median LLS. For comparison, for a spectral index of $\alpha = -0.8$, $\log P_{150}$ is larger by 0.62 and $\log P_{1400}$ is lower by 0.15 than our $\log P_{888}$.

Table 3. Comparison of six previous lists of GRS with our new sample.

(1) Surveys, Reference	(2) Freq. GHz	(3) N of GRS	(4) LAS '	(5) $S_{min,med}$ mJy	(6) $P_{min,med}$ W/Hz	(7) z_{med}	(8) f_{zsp}, f_{QSO}	(9) LLS Mpc
Literature [5]	0.8/1.4	223	6.7	9.2,154	23.4,25.5	0.23	0.89,0.17	1.41
LoTSS [15]	0.15	68	3.5	7.0,130	24.7,26.2	0.54	0.55,0.12	1.28
NVSS [59]	1.4	48	3.75	25,215	23.7,25.8	0.35	0.42,0.06	1.19
NVSS,FIRST [60]	1.4	18	5.0	6.0,40	23.5,24.8	0.22	1.0 ,0.0	1.18
ASKAP [16]	1.01	25	3.7	1.2,22	23.3,25.4	0.6	0.04,0.32	1.20
NVSS,SDSS [46]	1.4	76	2.7	—,—	25.3,26.0	0.82	0.97,1.00	1.22
RACS, this work	0.888	178	3.1	5.0,40	23.5,25.9	0.66	0.06,0.18	1.22

Table 3 shows, not surprisingly, that the literature compiled by [5] has the largest median LAS and LLS, while ours is the one with the second-smallest median LAS, only surpassed by [46], who performed a dedicated search for extended radio emission from spectroscopic QSOs from SDSS DR14Q. The latter is also the sample with the highest median host redshifts, followed by our present sample. The sample with the lowest minimum and median flux density is from ASKAP [16] with its much higher sensitivity.

In Figure 5 we present the distribution of spectral radio power at 888 MHz from our new GRS sample drawn from RACS, as a function of LLS in the left panel, and as a function of host redshift in the right panel. The left panel, also called the $P - D$ diagram is similar to that in Figure 5 of [5] except for our sample being smaller, such that any trend is washed out by the large dispersion in P_{888} . The right panel shows a clear trend of P_{888} rising with redshift for galaxies, likely due to Malmquist bias. The panel is similar to that of Figure 4 of [15] except for the fact that our sample fills in a lack of galaxies at $z \sim 1$, which is due to the deeper DES DR1 images used by us compared to the SDSS images used by [15]. The dedicated search for GRQs among $\sim 526,000$ SDSS DR14 QSOs by [46] had shown a weak trend for radio power to increase with a redshift for GRQs with $z \gtrsim 0.5$ out to $z \sim 2.5$. Such a trend cannot be seen in our much smaller sample due to the lack of known spectroscopic QSOs in our search area.

In Figure 6, we show the location of our newly found 178 GRS in the $LAS - z$ diagram, compared to the previously published 458 GRS, with reference lines drawn for “standard rulers” of four different sizes. The fact that no GRS larger than 5 Mpc has yet been found suggests that this may be a physical limit. The diagram also shows that GRS become much more numerous for smaller LLS, but for $LLS < 1$ Mpc, this has not been quantified in the literature as of yet. Figure 7 shows the very rapid decrease in the number of GRS larger than a given LLS as a function of LLS. The data in Figure 7 actually show a flatter slope of this relation of about -3.3 below ~ 2 Mpc, while above that size the slope is steeper than -4 . Below 1 Mpc, this slope becomes flatter: the number of ~ 300 GRS found by us with $LLS = 0.7-1.0$ Mpc, plus ~ 400 of $0.5-0.7$ Mpc, suggest slopes of -2.8 and -1.8 , respectively, for these latter size ranges. For the literature compiled by [5] with 136 GRS of $0.7 < LLS < 1.0$ Mpc, the slope in this LLS range is much flatter (-1.4), indicating that little attention had been paid to these smaller sources in the literature prior to this compilation.

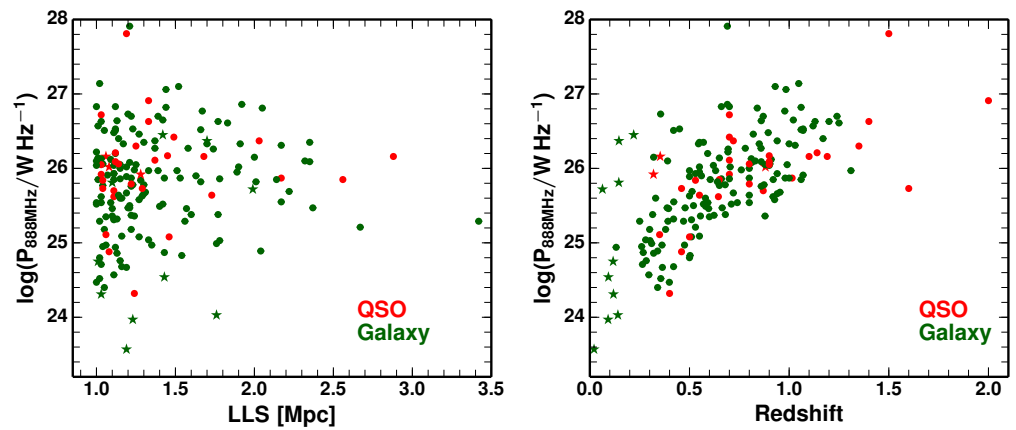


Figure 5. Spectral radio power P_{888} as function of LLS (left) and as a function of host redshift (right). Green filled circles are galaxies and red ones are QSOs or candidates with photometric redshifts, and star symbols indicate objects with spectroscopic redshifts.

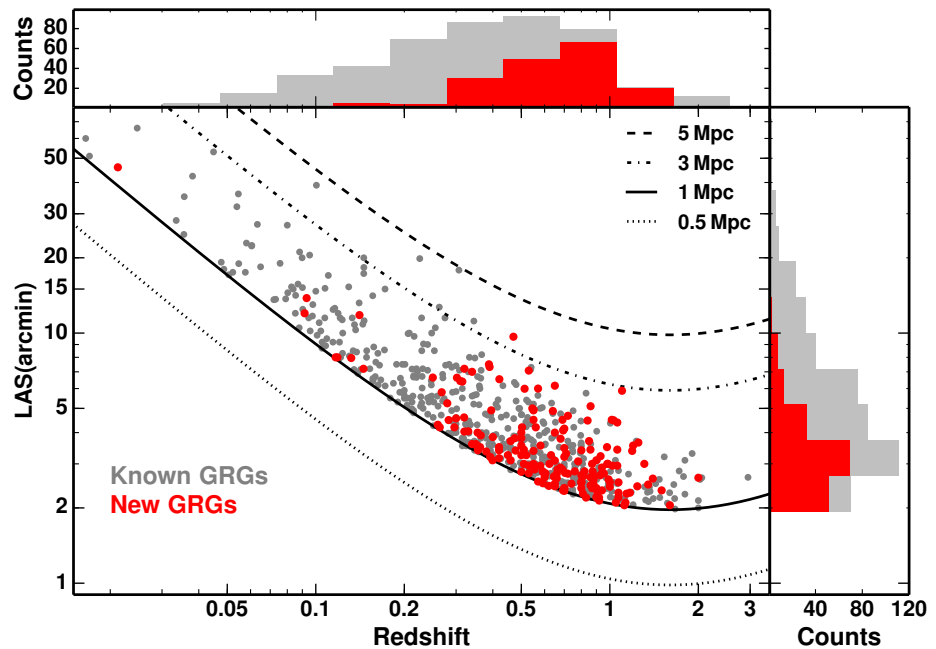


Figure 6. The location of GRG in a LAS–redshift diagram. The grey points indicate the 458 GRG from the six major literature compilations, and the red points those in our new sample. The LAS of four “standard rulers” of 0.5, 1, 3, and 5 Mpc are indicated by lines as described in the upper right corner of the diagram, assuming the cosmological parameters listed at the end of Section 1.

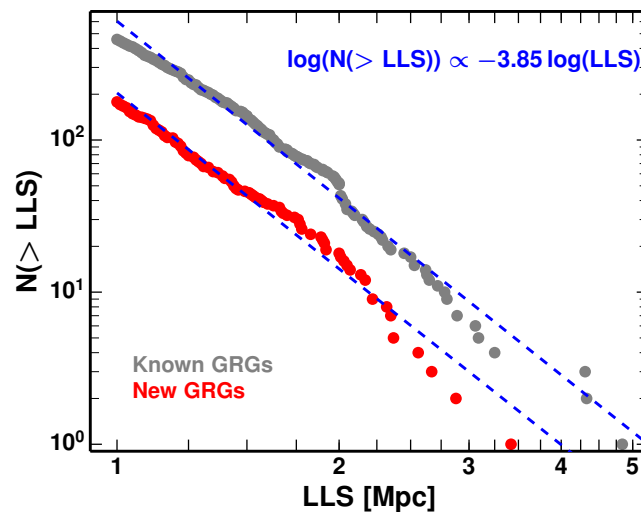


Figure 7. The grey and red dots indicate the number of known GRG from the six publications described in Section 4.1 and our 178 new GRG, respectively, larger than a given LLS, as function of LLS. The slopes fitted to the $\log N(>LLS)$ – $\log LLS$ relation for the known and new GRG are -3.86 ± 0.04 , and -3.84 ± 0.07 , respectively, and the dashed blue line is the average fit to both. The best-fit slope for the total population (not shown here) is -4.02 ± 0.04 .

4.2. Multi-Wavelength Counterparts of GRG Hosts from RACS

The use of the deep multi-band optical images from the Dark Energy Survey (DES DR1 [22]) brings a clear improvement over the use of previous shallower optical surveys such as the Digitized Sky Survey (DSS2, [37]) or SkyMapper (SMSS) DR1 [21]. In fact, only 86 (43%) of the 178 hosts of the new GRG are listed in the USNO B1.0 catalog drawn from the DSS images [92], and only 35 (19.6%) are found in the SMSS DR1 catalog. In contrast, 175 of the 178 new GRG hosts are found in the DES DR1 catalog [22], and of the remaining three, J0600–4908 and J2331–4928 are listed in the DESI DR9 catalogue ([42], <https://www.legacysurvey.org> (accessed on 20 September 2021), and J0131–4901 is recognized on DESI DR9 images but not cataloged, so we estimated its redshift.

On the other hand, the WISE-based object catalogs are also very efficient in detecting GRG hosts: 163 (91.6%) of the 178 new GRG hosts are detected in AllWISE [23], and 169 (96%) are detected in CatWISE2020 [49].

4.3. Comparison of RACS with SUMSS

The motivation for our effort to identify over 1400 extended radio sources on RACS was its three-times-better angular resolution of $\sim 15''$ compared to that of SUMSS ($45''$). However, we found that for sources with very large LAS of $\gtrsim 15'$ and very diffuse and low surface brightness lobes, SUMSS often traces these sources with higher fidelity. In Figure 8 we show one example of this by comparing the CRACS and SUMSS images of J0138–4231, the nearby galaxy NGC 641, where the RACS image is affected by streaks parallel to the inner jets and the SW lobe of the source, possibly due to the fact that ASKAP has a shortest baseline of 22 m [14] and RACS was observed with a short exposure time of 15 min, while SUMSS [19] required 12 h integrations for the East–West array with virtually zero minimum spacings. We added contours from GLEAM [77] on top of the SUMSS image, confirming the reality of the lobes. Another example for which we found the SUMSS image of better quality than RACS is J2226–4316, a $13.8'$ wide GRG of $LLS = 1.4$ Mpc hosted by the $z_{spec} = 0.0931$ galaxy 2MASX J22263358–4316356. The good sensitivity of SUMSS for low surface brightness extended sources is also borne out by the fact that 45 (25%) of the 178 newly found GRG were first seen on SUMSS images, only that the SUMSS angular resolution did not allow their secure optical identification.

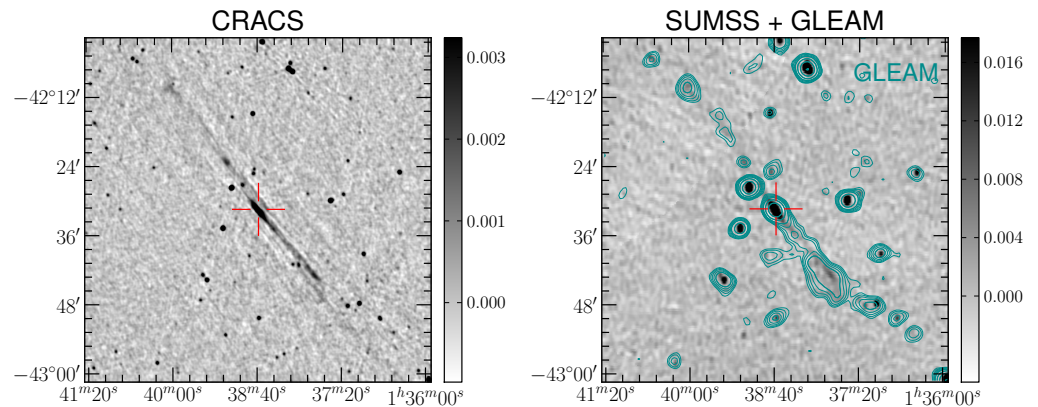


Figure 8. Radio images of J0138–4231 (NGC 641) from CRACS at 888 MHz (**left**) and SUMSS at 843 MHz (**right**), both in gray scale. The brightness levels in the scale bar on the right are in units of Jy beam^{-1} . The green contours in the right panel are from the GLEAM 170–231 MHz band at $\sim 2'$ resolution, plotted in the same sequence as in Figure 2 but with $\text{rms} = 5.5 \text{ mJy beam}^{-1}$. The gapped red crosses at the center mark the location of the host. See Section 4.3 for a discussion.

5. Summary and Future Prospects

We described the results of our search for radio sources extended by more than $\sim 1.4'$ on images of the RACS 888-MHz survey in a contiguous high-Galactic latitude ($|b| > 12.5^\circ$) area of 1059 deg^2 between declinations of -50° and -40° . A subsequent search for the optical host galaxies or quasars on color images of the Dark Energy Survey DR1 resulted in the identification of ~ 1000 such sources, and further use of available spectroscopic or photometric redshifts revealed that 178 of these are giant radio sources (GRS) larger than 1 Mpc in projection and previously unreported in literature. We thus increased the number of known GRS by $\sim 39\%$ from 458 to 636. To our knowledge, we present the largest sample of newly discovered GRS exceeding 1 Mpc in a single publication. We also demonstrated that the depth and angular resolution of RACS, together with deep optical/IR images, is perfectly suited for the identification of large RGs.

About 18% of the 178 new GRS are hosted by QSOs or QSO candidates, which is similar to previously published GRS lists (except for the dedicated search for GRQs by [46]). At least 10% of all GRS are hosted by brightest or other cluster galaxies. This fraction is a lower limit, since over half of our GRS lie at distances where cluster catalogues are still very incomplete.

Finding 178 GRS in 1059 deg^2 corresponds to a density of $\sim 0.17 \text{ deg}^{-2}$ in this area and confirms that RACS images have the potential of revealing ~ 5000 GRS over its entire survey area ($\text{Dec} < +41^\circ$). However, regions of low galactic latitude as well as regions not covered by the deepest optical surveys will yield a lower identification rate. On the other hand, the fact that RACS is being repeated at two higher frequencies (~ 1.2 and $\sim 1.6 \text{ GHz}$) will increase its sensitivity and potential for finding GRS.

We expect to double the present sample of GRS by inspecting the sky region from $\text{RA} = 20^h$ to $6^h 20^m$, and $-65^\circ < \text{Dec} < -50^\circ$, immediately south of that studied here, and also covered by DES and similar in size to the one just studied. Taken together, this promises a sample of over 350 GRS, plus ~ 600 sources with $\text{LLS} = 0.7\text{--}1 \text{ Mpc}$. However, the amount of work necessary to find new GRS is clearly impractical and calls for machine learning (ML) algorithms to find good candidates more efficiently. Samples such as the one presented in this work may serve as training sets for such algorithms.

Author Contributions: Conceptualization, H.A.; visual inspection of radio and optical images, data curation, statistical analysis, H.A.; radio-optical overlays and all graphics, E.F.J.-A.; software development for flux integration and determination of equipartition parameters, A.G.W.; writing, H.A., E.F.J.-A., A.G.W. All authors have read and agreed to the published version of the manuscript.

Funding: H.A. was partly funded by grant CIIC 174/2021 of DAIP, Univ. de Guanajuato, Mexico.

Institutional Review Board Statement: Not applicable.

Informed Consent Statement: Not applicable.

Data Availability Statement: All data used in this research are publicly available from sites quoted in the present paper. Table 2 will also be made available at the CDS and through the VizieR service. The list of radio galaxies smaller than 1 Mpc identified in the present work may be shared on reasonable request with researchers interested in collaborative projects.

Acknowledgments: In this work we have used data from the ASKAP observatory. The Australian SKA Pathfinder is part of the Australia Telescope National Facility, which is managed by CSIRO. Operation of ASKAP is funded by the Australian Government with support from the National Collaborative Research Infrastructure Strategy. ASKAP uses the resources of the Pawsey Supercomputing Center. Establishment of ASKAP, the Murchison Radio-astronomy Observatory, and the Pawsey Supercomputing Centre are initiatives of the Australian Government, with support from the Government of Western Australia and the Science and Industry Endowment Fund.

This research has made use of the VizieR catalog access tool, CDS, Strasbourg, France (DOI: 10.26093/cds/vizieR). The original description of the VizieR service was published in [47].

This research uses services or data provided by the Astro Data Lab at NSF's NOIRLab. NOIRLab is operated by the Association of Universities for Research in Astronomy (AURA), Inc. under a cooperative agreement with the National Science Foundation.

The DESI Legacy Surveys consist of three individual and complementary projects: the Dark Energy Camera Legacy Survey (DECaLS; Proposal ID #2014B-0404; PIs: David Schlegel and Arjun Dey), the Beijing-Arizona Sky Survey (BASS; NOAO Prop. ID #2015A-0801; PIs: Zhou Xu and Xiaohui Fan), and the Mayall z-band Legacy Survey (MzLS; Prop. ID #2016A-0453; PI: Arjun Dey). DECaLS, BASS, and MzLS together include data obtained, respectively, at the Blanco telescope, Cerro Tololo Inter-American Observatory, NSF's NOIRLab; the Bok telescope, Steward Observatory, University of Arizona; and the Mayall telescope, Kitt Peak National Observatory, NOIRLab. The Legacy Surveys project is honored to be permitted to conduct astronomical research on Iolkam Du'ag (Kitt Peak), a mountain with particular significance to the Tohono O'odham Nation.

The Photometric Redshifts for the Legacy Surveys (PRLS) catalog used in this paper was produced thanks to funding from the U.S. Department of Energy Office of Science, Office of High Energy Physics via grant DE-SC0007914.

Use was made of data products from the Wide-field Infrared Survey Explorer, which is a joint project of the University of California, Los Angeles, and the Jet Propulsion Laboratory/California Institute of Technology, funded by the National Aeronautics and Space Administration.

We also made use of data from the European Space Agency (ESA) mission *Gaia* (<https://www.cosmos.esa.int/gaia> (accessed on 15 August 2021)), processed by the *Gaia* Data Processing and Analysis Consortium (DPAC, <https://www.cosmos.esa.int/web/gaia/dpac/consortium> (accessed on 15 August 2021)). Funding for the DPAC has been provided by national institutions, in particular the institutions participating in the *Gaia* Multilateral Agreement.

This research has made use of the NASA/IPAC Extragalactic Database, which is funded by the National Aeronautics and Space Administration and operated by the California Institute of Technology.

We are grateful to Karla Alamo Martínez for help with extracting photometric redshifts from DESI DR9, Raúl F. Maldonado for his work in 2012 in spotting extended radio sources in SUMSS images, and to Irina Andernach for her help with optical identifications of RACS sources. We thank two anonymous referees for their useful comments.

Conflicts of Interest: The authors declare no conflict of interest.

Note

- ¹ Note that this galaxy does not have a z_{spec} , neither in [12] nor as claimed by NED, which quotes $z_{spec} = 0.093$ from [80], which is actually a z_{phot} . Simbad (<http://simbad.u-strasbg.fr> (accessed on 15 September 2021)) quotes $z_{spec} = 0.1021$ from [81], obtained from [82] who assigned this redshift to the cluster, but the redshift refers to another cluster member, and the radial velocity of $34,851 \text{ km s}^{-1}$ in [83] cannot be traced to any literature reference.

References

1. Willis, A.G.; Strom, R.G.; Wilson, A.S. 3C236, DA240; the largest radio sources known. *Nature* **1974**, *250*, 625–630. [CrossRef]
2. Hintzen, P.; Ulvestad, J.; Owen, F. Are wide-angle radio-tail QSOs members of clusters of galaxies? I. VLA maps at 20 CM of 117 radio quasars. *Astron. J.* **1983**, *88*, 709–758. [CrossRef]
3. Machalski, J.; Koziel-Wierzbowska, D.; Jamrozy, M.; Saikia, D.J. J1420-0545: The Radio Galaxy Larger than 3C 236. *Astrophys. J.* **2008**, *679*, 149–155. [CrossRef]
4. Coziol, R.; Andernach, H.; Torres-Papaqui, J.P.; Ortega-Minakata, R.A.; Moreno del Rio, F. What sparks the radio-loud phase of nearby quasars? *Mon. Not. R. Astron. Soc.* **2017**, *466*, 921–944. [CrossRef]
5. Kuźmicz, A.; Jamrozy, M.; Bronarska, K.; Janda-Boczar, K.; Saikia, D.J. An Updated Catalog of Giant Radio Sources. *Astrophys. J. Suppl.* **2018**, *238*, 9. [CrossRef]
6. Banfield, J.K.; Wong, O.I.; Willett, K.W.; Norris, R.P.; Rudnick, L.; Shabala, S.S.; Simmons, B.D.; Snyder, C.; Garon, A.; Seymour, N.; et al. Radio Galaxy Zoo: host galaxies and radio morphologies derived from visual inspection. *Mon. Not. R. Astron. Soc.* **2015**, *453*, 2326–2340. [CrossRef]
7. O’Sullivan, S.P.; Machalski, J.; Van Eck, C.L.; Heald, G.; Brügggen, M.; Fynbo, J.P.U.; Heintz, K.E.; Lara-Lopez, M.A.; Vacca, V.; Hardcastle, M.J.; et al. The intergalactic magnetic field probed by a giant radio galaxy. *Astron. Astrophys.* **2019**, *622*, A16. [CrossRef]
8. Bridle, A.H.; Davis, M.M.; Meloy, D.A.; Fomalont, E.B.; Strom, R.G.; Willis, A.G. Giant radio galaxy NGC 315. *Nature* **1976**, *262*, 179–182. [CrossRef]
9. Strom, R.G.; Willis, A.G.; Wilson, A.S. High resolution observations of large and complex radio galaxies. *Mem. Della Soc. Astron. Ital.* **1974**, *45*, 535.
10. Condon, J.J.; Cotton, W.D.; Greisen, E.W.; Yin, Q.F.; Perley, R.A.; Taylor, G.B.; Broderick, J.J. The NRAO VLA Sky Survey. *Astron. J.* **1998**, *115*, 1693–1716. [CrossRef]
11. Becker, R.H.; White, R.L.; Helfand, D.J. The FIRST Survey: Faint Images of the Radio Sky at Twenty Centimeters. *Astrophys. J.* **1995**, *450*, 559. [CrossRef]
12. Ahumada, R.; Prieto, C.A.; Almeida, A.; Anders, F.; Anderson, S.F.; Andrews, B.H.; Anguiano, B.; Arcodia, R.; Armengaud, E.; Aubert, M.; et al. The 16th Data Release of the Sloan Digital Sky Surveys: First Release from the APOGEE-2 Southern Survey and Full Release of eBOSS Spectra. *Astrophys. J. Suppl.* **2020**, *249*, 3. [CrossRef]
13. Shimwell, T.W.; Tasse, C.; Hardcastle, M.J.; Mechev, A.P.; Williams, W.L.; Best, P.N.; Röttgering, H.J.A.; Callingham, J.R.; Dijkema, T.J.; de Gasperin, F.; et al. The LOFAR Two-metre Sky Survey. II. First data release. *Astron. Astrophys.* **2019**, *622*, A1. [CrossRef]
14. Hotan, A.W.; Bunton, J.D.; Chippendale, A.P.; Whiting, M.; Tuthill, J.; Moss, V.A.; McConnell, D.; Amy, S.W.; Huynh, M.T.; Allison, J.R.; et al. Australian square kilometre array pathfinder: I. system description. *Publ. Astron. Soc. Aust.* **2021**, *38*, e009. [CrossRef]
15. Dabhade, P.; Röttgering, H.J.A.; Bagchi, J.; Shimwell, T.W.; Hardcastle, M.J.; Sankhyayan, S.; Morganti, R.; Jamrozy, M.; Shulevski, A.; Duncan, K.J. Giant radio galaxies in the LOFAR Two-metre Sky Survey. I. Radio and environmental properties. *Astron. Astrophys.* **2020**, *635*, A5. [CrossRef]
16. Brügggen, M.; Reiprich, T.H.; Bulbul, E.; Koribalski, B.S.; Andernach, H.; Rudnick, L.; Hoang, D.N.; Wilber, A.G.; Duchesne, S.W.; Veronica, A.; et al. Radio observations of the merging galaxy cluster system Abell 3391-Abell 3395. *Astron. Astrophys.* **2021**, *647*, A3. [CrossRef]
17. Norris, R.P.; Marvil, J.; Collier, J.D.; Kapińska, A.D.; O’Brien, A.N.; Rudnick, L.; Andernach, H.; Asorey, J.; Brown, M.J.I.; Brügggen, M.; et al. The Evolutionary Map of the Universe pilot survey. *Publ. Astron. Soc. Aust.* **2021**, *38*, e046. [CrossRef]
18. McConnell, D.; Hale, C.L.; Lenc, E.; Banfield, J.K.; Heald, G.; Hotan, A.W.; Leung, J.K.; Moss, V.A.; Murphy, T.; O’Brien, A.; et al. The Rapid ASKAP Continuum Survey I: Design and first results. *Publ. Astron. Soc. Aust.* **2020**, *37*, e048. [CrossRef]
19. Bock, D.C.J.; Large, M.I.; Sadler, E.M. SUMSS: A Wide-Field Radio Imaging Survey of the Southern Sky. I. Science Goals, Survey Design, and Instrumentation. *Astron. J.* **1999**, *117*, 1578–1593. [CrossRef]
20. Mauch, T.; Murphy, T.; Buttery, H.J.; Curran, J.; Hunstead, R.W.; Pietrzynski, B.; Robertson, J.G.; Sadler, E.M. SUMSS: A wide-field radio imaging survey of the southern sky-II. The source catalogue. *Mon. Not. R. Astron. Soc.* **2003**, *342*, 1117–1130. [CrossRef]
21. Wolf, C.; Onken, C.A.; Luvaul, L.C.; Schmidt, B.P.; Bessell, M.S.; Chang, S.W.; Da Costa, G.S.; Mackey, D.; Martin-Jones, T.; Murphy, S.J.; et al. SkyMapper Southern Survey: First Data Release (DR1). *Publ. Astron. Soc. Aust.* **2018**, *35*, e010. [CrossRef]
22. Abbott, T.M.C.; Abdalla, F.B.; Allam, S.; Amara, A.; Annis, J.; Asorey, J.; Avila, S.; Ballester, O.; Banerji, M.; Barkhouse, W.; et al. The Dark Energy Survey: Data Release 1. *Astrophys. J. Suppl.* **2018**, *239*, 18. [CrossRef]

23. Cutri, R.M.; Wright, E.L.; Conrow, T.; Fowler, J.W.; Eisenhardt, P.R.M.; Grillmair, C.; Kirkpatrick, J.D.; Masci, F.; McCallon, H.L.; Wheelock, S.L.; et al. Explanatory Supplement to the AllWISE Data Release Products. In *Explanatory Supplement to the AllWISE Data Release Products*; Infrared Science Archive: Pasadena, CA, USA, 2013. Available online: http://wise2.ipac.caltech.edu/docs/release/allwise/expsup/sec2_1a.html (accessed on 20 September 2021).
24. Lang, D. unWISE: Unblurred Coadds of the WISE Imaging. *Astron. J.* **2014**, *147*, 108. [[CrossRef](#)]
25. Komberg, B.V.; Pashchenko, I.N. Giant radio galaxies: Old long-lived quasars? *Astron. Rep.* **2009**, *53*, 1086–1100. [[CrossRef](#)]
26. Malarecki, J.M.; Staveley-Smith, L.; Saripalli, L.; Subrahmanyan, R.; Jones, D.H.; Duffy, A.R.; Rioja, M. Giant radio galaxies-I. Intergalactic barometers. *Mon. Not. R. Astron. Soc.* **2013**, *432*, 200–224. [[CrossRef](#)]
27. Malarecki, J.M.; Jones, D.H.; Saripalli, L.; Staveley-Smith, L.; Subrahmanyan, R. Giant radio galaxies-II. Tracers of large-scale structure. *Mon. Not. R. Astron. Soc.* **2015**, *449*, 955–986. [[CrossRef](#)]
28. Taylor, A.R.; Jagannathan, P. Alignments of radio galaxies in deep radio imaging of ELAIS N1. *Mon. Not. R. Astron. Soc.* **2016**, *459*, L36–L40. [[CrossRef](#)]
29. Contigiani, O.; de Gasperin, F.; Miley, G.K.; Rudnick, L.; Andernach, H.; Banfield, J.K.; Kapińska, A.D.; Shabala, S.S.; Wong, O.I. Radio Galaxy Zoo: cosmological alignment of radio sources. *Mon. Not. R. Astron. Soc.* **2017**, *472*, 636–646. [[CrossRef](#)]
30. Boyce, E. Giant Radio Galaxies. Honors Thesis, Sydney University, Sydney, Australia, 2000. Available online: http://www.astro.physics.usyd.edu.au/SUMSS/PAPERS/boyce_honours.pdf (accessed on 20 September 2021).
31. Saripalli, L.; Hunstead, R.W.; Subrahmanyan, R.; Boyce, E. A Complete Sample of Megaparsec-sized Double Radio Sources from the Sydney University Molonglo Sky Survey. *Astron. J.* **2005**, *130*, 896–922. [[CrossRef](#)]
32. Prandoni, I.; Gregorini, L.; Parma, P.; de Ruiter, H.R.; Vettolani, G.; Wieringa, M.H.; Ekers, R.D. The ATESP radio survey. II. The source catalogue. *Astron. Astrophys. Suppl.* **2000**, *146*, 41–55. [[CrossRef](#)]
33. Hopkins, A.M.; Mobasher, B.; Cram, L.; Rowan-Robinson, M. The PHOENIX Deep Survey: 1.4-GHz source counts. *Mon. Not. R. Astron. Soc.* **1998**, *296*, 839–846. [[CrossRef](#)]
34. Hopkins, A.M.; Afonso, J.; Chan, B.; Cram, L.E.; Georgakakis, A.; Mobasher, B. The Phoenix Deep Survey: The 1.4 GHz Microjansky Catalog. *Astron. J.* **2003**, *125*, 465–477. [[CrossRef](#)]
35. Hale, C.L.; McConnell, D.; Thomson, A.J.M.; Lenc, E.; Heald, G.H.; Hotan, A.W.; Leung, J.K.; Moss, V.A.; Murphy, T.; Pritchard, J.; et al. The Rapid ASKAP Continuum Survey Paper II: First Stokes I Source Catalogue Data Release. *arXiv* **2021**, arXiv:2109.00956.
36. Andernach, H.; Jiménez Andrade, E.F.; Maldonado Sánchez, R.F.; Vásquez Báez, I.R. Finding Giant Radio Galaxies in Imaging Radio Surveys. In *Science from the Next Generation Imaging and Spectroscopic Surveys*; European Southern Observatory: Garching, Germany, 2012; p. P1. Available online: <https://ui.adsabs.harvard.edu/abs/2012sngi.confP...1A> (accessed on 20 September 2021).
37. Lasker, B.M.; Doggett, J.; McLean, B.; Sturch, C.; Djorgovski, S.; de Carvalho, R.R.; Reid, I.N. The Palomar-ST ScI Digitized Sky Survey (POSS-II): Preliminary Data Availability. In *Astronomical Data Analysis Software and Systems V*; Jacoby, G.H., Barnes, J., Eds.; Astronomical Society of the Pacific Conference Series; Astronomical Society of the Pacific: San Francisco, CA, USA, 1996. Volume 101, p. 88.
38. Bonnarel, F.; Fernique, P.; Bienaimé, O.; Egret, D.; Genova, F.; Louys, M.; Ochsenbein, F.; Wenger, M.; Bartlett, J.G. The ALADIN interactive sky atlas. A reference tool for identification of astronomical sources. *Astron. Astrophys. Suppl.* **2000**, *143*, 33–40. [[CrossRef](#)]
39. Carroll, B.; Ostlie, D. *An Introduction to Modern Astrophysics*; Pearson New International, Ed.; Pearson Education Limited: Essex, UK, 2014.
40. Fanaroff, B.L.; Riley, J.M. The morphology of extragalactic radio sources of high and low luminosity. *Mon. Not. R. Astron. Soc.* **1974**, *167*, 31P–36P. [[CrossRef](#)]
41. de la Rosa Valdés, P.A.; Andernach, H. Statistics of Hotspots in Radio Galaxies. *arXiv* **2019**, arXiv:1908.09988.
42. Dey, A.; Schlegel, D.J.; Lang, D.; Blum, R.; Burleigh, K.; Fan, X.; Findlay, J.R.; Finkbeiner, D.; Herrera, D.; Juneau, S.; et al. Overview of the DESI Legacy Imaging Surveys. *Astron. J.* **2019**, *157*, 168. [[CrossRef](#)]
43. Brown, A.G.A.; Vallenari, A.; Prusti, T.; de Bruijne, J.H.J.; Babusiaux, C.; Biermann, M.; Creevey, O.L.; Evans, D.W.; Eyer, L.; Hutton, A.; et al. Gaia Early Data Release 3. Summary of the contents and survey properties. *Astron. Astrophys.* **2021**, *649*, A1. [[CrossRef](#)]
44. Nikutta, R.; Hunt-Walker, N.; Nenkova, M.; Ivezić, Ž.; Elitzur, M. The meaning of WISE colours-I. The Galaxy and its satellites. *Mon. Not. R. Astron. Soc.* **2014**, *442*, 3361–3379. [[CrossRef](#)]
45. Mao, M.Y.; Owen, F.; Duffin, R.; Keel, B.; Lacy, M.; Momjian, E.; Morrison, G.; Mroczkowski, T.; Neff, S.; Norris, R.P.; et al. J1649+2635: A grand-design spiral with a large double-lobed radio source. *Mon. Not. R. Astron. Soc.* **2015**, *446*, 4176–4185. [[CrossRef](#)]
46. Kuźmicz, A.; Jamroz, M. Giant Radio Quasars: Sample and Basic Properties. *Astrophys. J. Suppl.* **2021**, *253*, 25. [[CrossRef](#)]
47. Ochsenbein, F.; Bauer, P.; Marcout, J. The Vizier database of astronomical catalogues. *Astron. Astrophys. Suppl.* **2000**, *143*, 23–32. [[CrossRef](#)]
48. Skrutskie, M.F.; Cutri, R.M.; Stiening, R.; Weinberg, M.D.; Schneider, S.; Carpenter, J.M.; Beichman, C.; Capps, R.; Chester, T.; Elias, J.; et al. The Two Micron All Sky Survey (2MASS). *Astron. J.* **2006**, *131*, 1163–1183. [[CrossRef](#)]
49. Marocco, F.; Eisenhardt, P.R.M.; Fowler, J.W.; Kirkpatrick, J.D.; Meisner, A.M.; Schlafly, E.F.; Stanford, S.A.; Garcia, N.; Caselden, D.; Cushing, M.C.; et al. The CatWISE2020 Catalog. *Astrophys. J. Suppl.* **2021**, *253*, 8. [[CrossRef](#)]

50. Bilicki, M.; Jarrett, T.H.; Peacock, J.A.; Cluver, M.E.; Steward, L. Two Micron All Sky Survey Photometric Redshift Catalog: A Comprehensive Three-dimensional Census of the Whole Sky. *Astrophys. J. Suppl.* **2014**, *210*, 9. [[CrossRef](#)]
51. Bilicki, M.; Peacock, J.A.; Jarrett, T.H.; Cluver, M.E.; Maddox, N.; Brown, M.J.I.; Taylor, E.N.; Hambly, N.C.; Solarz, A.; Holwerda, B.W.; et al. WISE × SuperCOSMOS Photometric Redshift Catalog: 20 Million Galaxies over 3/pi Steradians. *Astrophys. J. Suppl.* **2016**, *225*, 5. [[CrossRef](#)]
52. Zhou, R.; Newman, J.A.; Mao, Y.Y.; Meisner, A.; Moustakas, J.; Myers, A.D.; Prakash, A.; Zentner, A.R.; Brooks, D.; Duan, Y.; et al. The clustering of DESI-like luminous red galaxies using photometric redshifts. *Mon. Not. R. Astron. Soc.* **2021**, *501*, 3309–3331. [[CrossRef](#)]
53. Flesch, E.W. The Million Quasars (Milliquas) v7.2 Catalogue, now with VLASS associations. The inclusion of SDSS-DR16Q quasars is detailed. *arXiv* **2021**, arXiv:2105.12985.
54. Krogager, J.K.; Gupta, N.; Noterdaeme, P.; Ranjan, A.; Fynbo, J.P.U.; Srianand, R.; Petitjean, P.; Combes, F.; Mahabal, A. MALS-NOT: Identifying Radio-bright Quasars for the MeerKAT Absorption Line Survey. *Astrophys. J. Suppl.* **2018**, *235*, 10. [[CrossRef](#)]
55. Wright, E.L. A Cosmology Calculator for the World Wide Web. *Publ. Astron. Soc. Pac.* **2006**, *118*, 1711–1715. [[CrossRef](#)]
56. Machalski, J.; Kozieł-Wierzbowska, D.; Goyal, A. An Atlas of Dynamical Evolution Models of 361 Fanaroff-Riley Type II Radio Sources. *Astrophys. J. Suppl.* **2021**, *255*, 22. [[CrossRef](#)]
57. Miley, G. The structure of extended extragalactic radio sources. *Annu. Rev. Astron. Astrophys.* **1980**, *18*, 165–218. [[CrossRef](#)]
58. Jackson, C.A.; Wall, J.V. Radio Galaxy Spectra. In *Particles and Fields in Radio Galaxies Conference*; Laing, R.A., Blundell, K.M., Eds.; Astronomical Society of the Pacific Conference Series; Astronomical Society of the Pacific: San Francisco, CA, USA, 2001; Volume 250, p. 400.
59. Dabhade, P.; Mahato, M.; Bagchi, J.; Saikia, D.J.; Combes, F.; Sankhyayan, S.; Röttgering, H.J.A.; Ho, L.C.; Gaikwad, M.; Raychaudhury, S.; et al. Search and analysis of giant radio galaxies with associated nuclei (SAGAN). I. New sample and multi-wavelength studies. *Astron. Astrophys.* **2020**, *642*, A153. [[CrossRef](#)]
60. Kozieł-Wierzbowska, D.; Goyal, A.; Żywucka, N. Radio Sources Associated with Optical Galaxies and Having Unresolved or Extended Morphologies (ROGUE). I. A Catalog of SDSS Galaxies with FIRST Core Identifications. *Astrophys. J. Suppl.* **2020**, *247*, 53. [[CrossRef](#)]
61. Burgess, A.M.; Hunstead, R.W. The Molonglo Southern 4 Jy Sample (MS4). II. ATCA Imaging and Optical Identification. *Astron. J.* **2006**, *131*, 114–132. [[CrossRef](#)]
62. Colless, M.; Dalton, G.; Maddox, S.; Sutherland, W.; Norberg, P.; Cole, S.; Bland-Hawthorn, J.; Bridges, T.; Cannon, R.; Collins, C.; et al. The 2dF Galaxy Redshift Survey: spectra and redshifts. *Mon. Not. R. Astron. Soc.* **2001**, *328*, 1039–1063. [[CrossRef](#)]
63. Jones, P.A.; McAdam, W.B. The Structure of Southern Extragalactic Radio Sources. *Astrophys. J. Suppl.* **1992**, *80*, 137. [[CrossRef](#)]
64. Jones, D.H.; Read, M.A.; Saunders, W.; Colless, M.; Jarrett, T.; Parker, Q.A.; Fairall, A.P.; Mauch, T.; Sadler, E.M.; Watson, F.G.; et al. The 6dF Galaxy Survey: final redshift release (DR3) and southern large-scale structures. *Mon. Not. R. Astron. Soc.* **2009**, *399*, 683–698. [[CrossRef](#)]
65. Danziger, I.J.; Goss, W.M.; Frater, R.H. The giant radio galaxies PKS 0211-47 and PKS 0634-20. *Mon. Not. R. Astron. Soc.* **1978**, *184*, 341–349. [[CrossRef](#)]
66. Danziger, I.J.; Goss, W.M. Optical spectroscopy of 28 southern radio galaxies. *Mon. Not. R. Astron. Soc.* **1983**, *202*, 703–715. [[CrossRef](#)]
67. Loveday, J.; Peterson, B.A.; Maddox, S.J.; Efstathiou, G. The Stromlo-APM Redshift Survey. IV. The Redshift Catalog. *Astrophys. J. Suppl.* **1996**, *107*, 201. [[CrossRef](#)]
68. Wisotzki, L.; Christlieb, N.; Bade, N.; Beckmann, V.; Köhler, T.; Vanelle, C.; Reimers, D. The Hamburg/ESO survey for bright QSOs. III. A large flux-limited sample of QSOs. *Astron. Astrophys.* **2000**, *358*, 77–87.
69. Shu, Y.; Kopylov, S.E.; Evans, N.W.; Belokurov, V.; McMahon, R.G.; Auger, M.W.; Lemon, C.A. Catalogues of active galactic nuclei from Gaia and unWISE data. *Mon. Not. R. Astron. Soc.* **2019**, *489*, 4741–4759. [[CrossRef](#)]
70. Kapińska, A.D.; Terentev, I.; Wong, O.I.; Shabala, S.S.; Andernach, H.; Rudnick, L.; Storer, L.; Banfield, J.K.; Willett, K.W.; de Gasperin, F.; et al. Radio Galaxy Zoo: A Search for Hybrid Morphology Radio Galaxies. *Astron. J.* **2017**, *154*, 253. [[CrossRef](#)]
71. Norris, R.P.; Intema, H.T.; Kapińska, A.D.; Koribalski, B.S.; Lenc, E.; Rudnick, L.; Alsaberi, R.Z.E.; Anderson, C.; Anderson, G.E.; Crawford, E.; et al. Unexpected circular radio objects at high Galactic latitude. *Publ. Astron. Soc. Aust.* **2021**, *38*, e003. [[CrossRef](#)]
72. Owen, F.N.; White, R.A. Surface photometry of radio galaxies. II. Cluster sources. *Mon. Not. R. Astron. Soc.* **1991**, *249*, 164. [[CrossRef](#)]
73. Owen, F.N.; Ledlow, M.J. The FRI/II Break and the Bivariate Luminosity Function in Abell Clusters of Galaxies. In *The Physics of Active Galaxies*; Bicknell, G.V., Dopita, M.A., Quinn, P.J., Eds.; Astronomical Society of the Pacific Conference Series; Astronomical Society of the Pacific: San Francisco, CA, USA, 1994; Volume 54, p. 319.
74. Best, P.N. Radio source populations: Results from SDSS. *Astron. Nachrichten* **2009**, *330*, 184–189. [[CrossRef](#)]
75. Mingo, B.; Croston, J.H.; Hardcastle, M.J.; Best, P.N.; Duncan, K.J.; Morganti, R.; Röttgering, H.J.A.; Sabater, J.; Shimwell, T.W.; Williams, W.L.; et al. Revisiting the Fanaroff-Riley dichotomy and radio-galaxy morphology with the LOFAR Two-Metre Sky Survey (LoTSS). *Mon. Not. R. Astron. Soc.* **2019**, *488*, 2701–2721. [[CrossRef](#)]
76. Owen, F.N. Steps Toward a Radio H-R Diagram. In *Jets in Extragalactic Radio Sources*; Röser, H.J., Meisenheimer, K., Eds.; Springer: Berlin, Germany, 1993. [[CrossRef](#)]

77. Hurley-Walker, N.; Callingham, J.R.; Hancock, P.J.; Franzen, T.M.O.; Hindson, L.; Kapińska, A.D.; Morgan, J.; Offringa, A.R.; Wayth, R.B.; Wu, C.; et al. GaLactic and Extragalactic All-sky Murchison Widefield Array (GLEAM) survey-I. A low-frequency extragalactic catalogue. *Mon. Not. R. Astron. Soc.* **2017**, *464*, 1146–1167. [[CrossRef](#)]
78. Zou, H.; Gao, J.; Xu, X.; Zhou, X.; Ma, J.; Zhou, Z.; Zhang, T.; Nie, J.; Wang, J.; Xue, S. Galaxy Clusters from the DESI Legacy Imaging Surveys. I. Cluster Detection. *Astrophys. J. Suppl.* **2021**, *253*, 56. [[CrossRef](#)]
79. Aguena, M.; Benoist, C.; da Costa, L.N.; Ogando, R.L.C.; Gschwend, J.; Sampaio-Santos, H.B.; Lima, M.; Maia, M.A.G.; Allam, S.; Avila, S.; et al. The WaZP galaxy cluster sample of the dark energy survey year 1. *Mon. Not. R. Astron. Soc.* **2021**, *502*, 4435–4456. [[CrossRef](#)]
80. Dabhade, P.; Gaikwad, M.; Bagchi, J.; Pandey-Pommier, M.; Sankhyayan, S.; Raychaudhury, S. Discovery of giant radio galaxies from NVSS: radio and infrared properties. *Mon. Not. R. Astron. Soc.* **2017**, *469*, 2886–2906. [[CrossRef](#)]
81. Yuan, Z.S.; Han, J.L.; Wen, Z.L. Radio luminosity function of brightest cluster galaxies. *Mon. Not. R. Astron. Soc.* **2016**, *460*, 3669–3678. [[CrossRef](#)]
82. Wen, Z.L.; Han, J.L. Calibration of the Optical Mass Proxy for Clusters of Galaxies and an Update of the WHL12 Cluster Catalog. *Astrophys. J.* **2015**, *807*, 178. [[CrossRef](#)]
83. Condon, J.J.; Matthews, A.M.; Broderick, J.J. Radio Sources in the Nearby Universe. *Astrophys. J.* **2019**, *872*, 148. [[CrossRef](#)]
84. Capetti, A.; Massaro, F.; Baldi, R.D. FRICAT: A FIRST catalog of FR I radio galaxies. *Astron. Astrophys.* **2017**, *598*, A49. [[CrossRef](#)]
85. Tasse, C.; Shimwell, T.; Hardcastle, M.J.; O’Sullivan, S.P.; van Weeren, R.; Best, P.N.; Bester, L.; Hugo, B.; Smirnov, O.; Sabater, J.; et al. The LOFAR Two-meter Sky Survey: Deep Fields Data Release 1. I. Direction-dependent calibration and imaging. *Astron. Astrophys.* **2021**, *648*, A1. [[CrossRef](#)]
86. Wen, Z.L.; Han, J.L.; Yang, F. A catalogue of clusters of galaxies identified from all sky surveys of 2MASS, WISE, and SuperCOSMOS. *Mon. Not. R. Astron. Soc.* **2018**, *475*, 343–352. [[CrossRef](#)]
87. Mahatma, V.H.; Hardcastle, M.J.; Williams, W.L.; Brienza, M.; Brügger, M.; Croston, J.H.; Gurkan, G.; Harwood, J.J.; Kunert-Bajraszewska, M.; Morganti, R.; et al. Remnant radio-loud AGN in the Herschel-ATLAS field. *Mon. Not. R. Astron. Soc.* **2018**, *475*, 4557–4578. [[CrossRef](#)]
88. Jurlin, N.; Morganti, R.; Brienza, M.; Mandal, S.; Maddox, N.; Duncan, K.J.; Shabala, S.S.; Hardcastle, M.J.; Prandoni, I.; Röttgering, H.J.A.; et al. The life cycle of radio galaxies in the LOFAR Lockman Hole field. *Astron. Astrophys.* **2020**, *638*, A34. [[CrossRef](#)]
89. Quici, B.; Hurley-Walker, N.; Seymour, N.; Turner, R.J.; Shabala, S.S.; Huynh, M.; Andernach, H.; Kapińska, A.D.; Collier, J.D.; Johnston-Hollitt, M.; et al. Remnant radio galaxies discovered in a multi-frequency survey. *Publ. Astron. Soc. Aust.* **2021**, *38*, e008. [[CrossRef](#)]
90. Saripalli, L.; Subrahmanyan, R.; Hunstead, R.W. 0319-454 : An FR II giant radio galaxy with twin jets. *Mon. Not. R. Astron. Soc.* **1994**, *269*, 37–51. [[CrossRef](#)]
91. Subrahmanyan, R.; Saripalli, L.; Hunstead, R.W. Morphologies in megaparsec-size powerful radio galaxies. *Mon. Not. R. Astron. Soc.* **1996**, *279*, 257–274. [[CrossRef](#)]
92. Monet, D.G.; Levine, S.E.; Canzian, B.; Ables, H.D.; Bird, A.R.; Dahn, C.C.; Guetter, H.H.; Harris, H.C.; Henden, A.A.; Leggett, S.K.; et al. The USNO-B Catalog. *Astron. J.* **2003**, *125*, 984–993. [[CrossRef](#)]